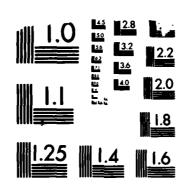STUDY OF DEFECTS PRODUCED BY THE GROWTH POST TREATMENT
AND FABRICATION OF... (U) OKLAHOMA STATE UNIV STILLWATER
DEPT OF PHYSICS L E HALLIBURTON ET AL. OCT 83
UNCLASSIFIED RADC-TR-83-231 F19628-80-C-0067   F/G 20/2   NL

MICROCOPY RESOLUTION TEST CHART

NATIONAL BUREAU OF STANDARDS-1963-A

RADC-TR-83-231
Final Technical Report
October 1983

STUDY OF DEFECTS PRODUCED BY THE GROWTH, POST TREATMENT AND FABRICATION OF QUARTZ

Oklahoma State University

Larry E. Halliburton
Joel J. Martin
William A. Sibley

APPROVED FOR PUBLIC RELEASE; DISTRIBUTION UNLIMITED

FEB 2 8 1984

A

ROME AIR DEVELOPMENT CENTER
Air Force Systems Command
Griffiss Air Force Base, NY 13441

AD A138327

DTIC FILE COPY

84   02   28   01

This report has been reviewed by the RADC Public Affairs Office (PA) and is releasable to the National Technical Information Service (NTIS). At NTIS it will be releasable to the general public, including foreign nations.

RADC-TR-83-231 has been reviewed and is approved for publication.

APPROVED: *Alton F. Armington*

ALTON F. ARMINGTON
Project Engineer

APPROVED: *Harold Roth*

HAROLD ROTH, Director
Solid State Sciences Division

FOR THE COMMANDER: *John A. Ritz*

JOHN A. RITZ
Acting Chief, Plans Office

REPORT DOCUMENTATION PAGE	READ INSTRUCTIONS BEFORE COMPLETING FORM

1. REPORT NUMBER	2. GOVT ACCESSION NO.	3. RECIPIENT'S CATALOG NUMBER
RADC-TR-83-231	AD-A138 327	

4. TITLE (and Subtitle)	5. TYPE OF REPORT & PERIOD COVERED
STUDY OF DEFECTS PRODUCED BY THE GROWTH, POST TREATMENT AND FABRICATION OF QUARTZ	Final Technical Report 15 Apr 80 – 30 Jun 83
	6. PERFORMING ORG. REPORT NUMBER
	N/A

7. AUTHOR(s)	8. CONTRACT OR GRANT NUMBER(s)
Larry E. Halliburton Joel J. Martin William A. Sibley	F19628-80-C-0067

9. PERFORMING ORGANIZATION NAME AND ADDRESS	10. PROGRAM ELEMENT, PROJECT, TASK AREA & WORK UNIT NUMBERS
Oklahoma State University Physics Department Stillwater OK 74074	61102F 2306J135

11. CONTROLLING OFFICE NAME AND ADDRESS	12. REPORT DATE
Rome Air Development Center (ESM) Hanscom AFB MA 01731.	October 1983
	13. NUMBER OF PAGES
	136

14. MONITORING AGENCY NAME & ADDRESS(If different from Controlling Office)	15. SECURITY CLASS. (of this report)
Same	UNCLASSIFIED
	15a. DECLASSIFICATION/DOWNGRADING SCHEDULE
	N/A

16. DISTRIBUTION STATEMENT (of this Report)

Approved for public release; distribution unlimited.

17. DISTRIBUTION STATEMENT (of the abstract entered in Block 20, if different from Report)

Same

18. SUPPLEMENTARY NOTES

RADC Project Engineer: Alton F. Armington (ESM)

19. KEY WORDS (Continue on reverse side if necessary and identify by block number)

Quartz crystals	ESR	E' Center
Radiation Damage	Electrolysis	Thermoluminescence
Q^{-1} Measurements	Aluminum-Hole Center	
Infrared Absorption	Electron Center	

20. ABSTRACT (Continue on reverse side if necessary and identify by block number)

In order to better understand the electrodiffusion process, we have systematically investigated various aspects of sweeping. Current-versus-time curves show an initial decay followed by a steady current. We believe that this steady current represents the migration of only one species of ion through the crystal. Once this steady state is reached, the temperature is slowly lowered and the ionic conductivity is measured versus temperature to obtain the activation energy. Alkalis show activa-

DD FORM 1473 EDITION OF 1 NOV 65 IS OBSOLETE

tion energies between .76 and 1.24 eV, while hydrogen shows an activation energy of 1.5 to 1.9 eV. Low-temperature IR absorption spectra, ESR spectra, and acoustic loss measurements were used to characterize the effects on the point defects of alkali and hydrogen electrodiffusion. Four-point bend fracture tests were carried out on a series of AT-cut samples as a function of etching and hydrogen sweeping. Etched samples from hydrogen-swept bars showed a greater fracture strength (i.e., were more difficult to fracture) than etched samples from similar unswept bars.

A study of the acoustic loss spectra of a series of 5 MHz 5th overtone AT-cut resonator blanks, all fabricated from the same bar of Premium Q grade quartz, as a function of electrodiffusion and irradiation has been completed. No acoustic loss peaks were observed at temperatures less than $100^\circ C$ which could be attributed to the $Al-OH^-$ or $AL-Li^+$ centers. Sodium-swept samples show a very large loss peak at 53 K while unswept samples have only a small 53 K peak. This shows, at least in as-grown Premium Q grade material, that most of the Al sites are compensated by Li^+ ions. Irradiation at room temperature removed the 53 K $Al-Na^+$ loss peak and produced three peaks (at 23 K, 100 K, and 135 K). Isochronal anneal studies show that all three of these radiation-induced loss peaks are caused by the Al-hole center. The isochronal anneal of the Na-Swept sample shows that the thermal decay of the Al-hole centers near 550 K is closely matched by a partial recovery of the $Al-Na^+$ center. The remaining recovery of the $Al-Na^+$ center takes place when the $Al-OH^-$ center goes out.

An electron-nuclear double resonance (ENDOR) study of the ^{27}Al Hyperfine and quadrupole interactions from the Al-hole, $(AlO_4)^0$, center has been completed. The anisotropic portion of the ^{27}Al hyperfine interaction has been analyzed in terms of contributions from both simple dipole-dipole effects and unpaired spin density in the 3p orbitals of the aluminum impurity ion.

Oxygen-vacancy-associated centers form an important class of defects in alpha-quartz. They are usually referred to as E centers, with E_1', E_2', E_4', E_1'', E_2'', and E_3'' centers being the ESR-active members of this family of defects. The single or double prime as a superscript denotes whether there are one or two unpaired electrons associated with the specific defect and the subscripts distinguish between various centers having each spin. We have surveyed the current status of defect models for these centers in alpha-quartz. Specific attention is given to the E_1', and E_4', and the three E'' centers. Brief consideration is also given to the origins of the ultraviolet (190 to 300 nm range) absorption bands in quartz.

The radiation-induced release of the charge compensating ions Li^+ and Na^+ from the substitutional aluminum impurity in quartz has been investigated by measuring the growth of the infrared-active $Al-OH^-$ center as a function of sample temperature during irradiation. It was found that Li^+ is released 10-15 K lower in temperature than Na^+.

Thermally stimulated luminescence (TSL) from one natural and two synthetic samples of alpha-quartz has been investigated in the range from room temperature to 400°C. Comparisons were made between unswept samples and others, taken from adjacent positions in the original stones, that were swept in a hydrogen atmosphere. Three sets of TSL data were obtained from each sample; corresponding to initial electron irradiation at 77 K, at ice-bath temperature, and a double irradiation at ice-path plus 77 K. Electron spin resonance (ESR) and infrared absorption (IR) data also were obtained from the same samples. A number of TSL peaks were found in the 60°C to 130°C region and they have been tentatively associated with hydrogen in the crystal. More intense peaks were found in the 200°C to 300°C region, but only in unswept samples after an ice-bath or ice-bath plus 77 K irradiation. These latter peaks are attributed to electron-hole recombination at $(AlO_4)^0$ centers as a result of electron release from alkali-associated electron traps.

Samples from approximately 20 RADC-grown quartz stones have been characterized by our ESR test for aluminum content. Pure Z-growth samples from several stones showed less than 1 ppm aluminum.
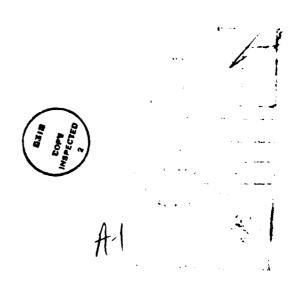
A-1

TABLE OF CONTENTS

[References, tables, and figures are numbered separately for each
section.]

I. INTRODUCTION AND SUMMARY

The defect structures in crystalline SiO_2, better known as quartz, and in related materials continue to be of considerable interest. Alpha-quartz, which is piezoelectric, finds application in a variety of electronic devices (e.g., high precision oscillators, filters, accelerometers, etc.) where stability and sensitivity are crucial operating criteria. However, a number of problems confront the systems designer when attempting to incorporate such precision frequency control devices into operational units. For example, in the case of quartz-controlled clocks, a major consideration is long term stability. Frequency shifts due to aging can disable an entire system. Equally important, quartz oscillators flown on satellites may experience low-level radiation which causes frequency shifts and alters the aging characteristics. The radiation response and, most likely, part of the aging of quartz crystals are related to the defects produced during crystal growth or during subsequent treatment.

Electrodiffusion (sweeping) is a post-growth treatment which allows the selective exchange of charge compensating interstitial ions in quartz. This technique is employed commercially to enhance the radiation hardness of the material used for quartz oscillator crystals. Nearly all quartz contains Al^{3+} ions substituting for Si^{4+}. Adjacent interstitial alkali ions or protons provide the necessary charge compensation for these Al^{3+} ions. Additional unidentified sites also trap protons to form the OH^--related defects which are responsible for several IR

absorption bands. When thermally released from their trapping sites, the interstitials can migrate along the relatively large Z axis channels. Therefore, if the sample is heated with an electric field applied along the Z axis, the ions can be swept out and replaced either by protons from the surrounding atmosphere or by the desired alkali from a salt electrode. This process also modifies extended defects, i.e., the etch tunnel density is reduced in hydrogen-swept material.

In order to better understand the electrodiffusion process, we have systematically investigated various aspects of sweeping. Current-versus-time curves show an initial decay followed by a steady current. We believe that this steady current represents the migration of only one species of ion through the crystal. Once this steady state is reached, the temperature is slowly lowered and the ionic conductivity is measured versus temperature to obtain the activation energy. Alkalis show activation energies between .76 and 1.24 eV, while hydrogen shows an activation energy of 1.5 to 1.9 eV. Low-temperature IR absorption spectra, ESR spectra, and acoustic loss measurements were used to characterize the effects on the point defects of alkali and hydrogen electrodiffusion. Four-point bend fracture tests were carried out on a series of AT-cut samples as a function of etching and hydrogen sweeping. Etched samples from hydrogen-swept bars showed a greater fracture strength (i.e., were more difficult to fracture) than etched samples from similar unswept bars.

A study of the acoustic loss spectra of a series of 5 MHz

5th overtone AT-cut resonator blanks, all fabricated from the same bar of Premium Q grade quartz, as a function of electrodiffusion and irradiation has been completed. No acoustic loss peaks were observed at temperatures less than 100°C which could be attributed to the Al-OH⁻ or Al-Li⁺ centers. Sodium-swept samples show a very large loss peak at 53 K while unswept samples have only a small 53 K peak. This shows, at least in as-grown Premium Q grade material, that most of the Al sites are compensated by Li^+ ions. Irradiation at room temperature removed the 53 K $Al-Na^+$ loss peak and produced three peaks (at 23 K, 100 K, and 135 K). Isochronal anneal studies show that all three of these radiation-induced loss peaks are caused by the Al-hole center. The isochronal anneal of the Na-swept sample shows that the thermal decay of the Al-hole centers near 550 K is closely matched by a partial recovery of the $Al-Na^+$ center. The remaining recovery of the $Al-Na^+$ center takes place when the Al-OH⁻ center goes out.

An electron-nuclear double resonance (ENDOR) study of the ^{27}Al hyperfine and quadrupole interactions from the Al-hole, $[AlO_4]^0$, center has been completed. The anisotropic portion of the ^{27}Al hyperfine interaction has been analyzed in terms of contributions from both simple dipole-dipole effects and unpaired spin density in the 3p orbitals of the aluminum impurity ion.

Oxygen-vacancy-associated centers form an important class of defects in alpha-quartz. They are usually referred to as E centers, with E_1', E_2', E_4', E_1'', E_2'', and E_3'' centers being the ESR-active members of this family of defects. The single or double prime as a superscript denotes whether there are one or two

3

unpaired electrons associated with the specific defect and the subscripts distinguish between various centers having each spin. We have surveyed the current status of defect models for these centers in alpha-quartz. Specific attention is given to the E_1', the E_4', and the three E'' centers. Brief consideration is also given to the origins of the ultraviolet (190 to 300 nm range) absorption bands in quartz.

The radiation-induced release of the charge compensating ions Li^+ and Na^+ from the substitutional aluminum impurity in - quartz has been investigated by measuring the growth of the infrared-active $Al-OH^-$ center as a function of sample temperature during irradiation. It was found that Li^+ is released 10-15 K lower in temperature than Na^+.

Thermally stimulated luminescence (TSL) from one natural and two synthetic samples of alpha-quartz has been investigated in the range from room temperature to 400°C. Comparisons were made between unswept samples and others, taken from adjacent positions in the original stones, that were swept in a hydrogen atmosphere. Three sets of TSL data were obtained from each sample; corresponding to initial electron irradiation at 77 K, at ice-bath temperature, and a double irradiation at ice-bath plus 77 K. Electron spin resonance (ESR) and infrared absorption (IR) data also were obtained from the same samples. A number of TSL peaks were found in the 60°C to 130°C region and they have been tentatively associated with hydrogen in the crystal. More intense peaks were found in the 200°C to 300°C region, but only in unswept samples after an ice-bath or ice-bath plus 77 K

4

irradiation. These latter peaks are attributed to electron-hole recombination at $[AlO_4]^O$ centers as a result of electron release from alkali-associated electron traps.

Samples from approximately 20 RADC-grown quartz stones have been characterized by our ESR test for aluminum content. Pure z-growth samples from several stones showed less than 1 ppm aluminum.

II. ELECTRODIFFUSION OF CHARGE-COMPENSATING IONS
IN ALPHA-QUARTZ

Introduction

Interstitial alkalis and protons can be trapped by substitutional aluminum ions[1] and other point defects in alpha-quartz. When liberated from such traps, either thermally or by radiation, the interstitial ions drift along the relatively large Z axis channels. This interstitial diffusion is responsible for the radiation-induced transient acoustic loss,[2] the increasing acoustic loss observed at high temperatures,[3-5] and the annealing of radiation-induced defects. An electric field applied parallel to the Z axis can be used at high temperatures to electrodiffuse (i.e., sweep) interstitial ions out of a sample and replace them with other ions.

King[6] was among the first to develop electrodiffusion as a method for changing the concentration of specific interstitial ions within a crystal. As part of his extensive infrared study, Kats[7] used the process to sweep specific alkalis and protons into and out of quartz. Fraser[8] has described the basic process for the selective electrodiffusion of alkalis and Krefft[9] has shown that holes can be swept into quartz if the process is carried out in vacuum above the phase transition. Alkali sweeping and the use of inert-gas atmospheres have been investigated by Brown, O'Conner, and Armington.[10] A number of studies have shown that the radiation hardness of oscillators is significantly enhanced if electrodiffusion has replaced the alkalis in the quartz with

protons.[11-13]

Arnold[14] has reported that etching quartz produces very deep tunnels while Nielsen and Foster[15] have observed that these tunnels tend to lie along the general growth direction. The tunnels are apparently caused by dislocation networks which trap impurities.[16] Vig et al.,[17] in a recent investigation of chemically polished and mechanically polished resonator blanks, found that swept material showed fewer of these etch tunnels and that chemically polished blanks were superior in strength.

Electrodiffusion is closely related to ionic conductivity. The main difference is the exchange of ions that takes place in the electrodiffusion process, i.e., specific ions (protons or alkalis) are brought into the sample to replace interstitial alkalis that had been trapped at defects during the crystal growth process. Electrical conductivity in quartz is ionic and one dimensional with monovalent ions moving along the Z axis channels. The number of mobile ions is governed by the number of traps, such as substitutional aluminum. If only one kind of trap, say aluminum, and one species of interstitials are present, the number of mobile ions per unit volume should be given by

$$n = (C_T/2)^{1/2} N_O \exp(-E_A/2kT) \qquad (1)$$

where C_T is the mole fraction of traps, N_O is the number of SiO_2's per unit volume, and E_A is the association energy between the ion and the trap.[18] The ion mobility[19] is given by

7

$$\mu = \frac{ed^2}{kT} \nu \, exp\left(-E_m / kT\right) \tag{2}$$

where d is the jump distance, ν is the jump frequency, and E_m is the activation energy for interstitial migration. Thus, the conductivity $\sigma = ne\mu$ can be expressed as

$$\sigma T = A \exp(-E/kT) \tag{3}$$

where

$$E = E_m + (1/2)E_A \tag{4}$$

and

$$A = \frac{N_o \, e \, d^2 \, \nu \, (C_T/2)^{1/2}}{kT} \tag{5}$$

According to this analysis, a plot of log σT versus T^{-1} should yield a straight line. Jain and Nowick[20] have reported such behavior and have found activation energies, E, near 1.4 and 1.0 eV for synthetic and natural quartz, respectively. The electrodiffusion process is expected to be more complicated since ion exchange is involved; however, Martin et al.[21] found a similar behavior for the ionic currents once the sweeping process has neared completion.

A systematic study of the electrodiffusion process in quartz is underway at Oklahoma State University. In addition to the effects of electrodiffusion on the point defects, we are also investigating the effects of sweeping on extended defects and

8

fracture in quartz.

Experimental Procedure

The samples used in this study were cut from unswept pure Z-growth lumbered bars of synthetic quartz. These bars included material from Thermodynamics, Sawyer Research Products (Electronic, Premium Q, and Super Premium Q grades), and an aluminum-doped synthetic bar. The various samples were identified according to the notation established by Markes and Halliburton.[22] Z plates 3 mm thick and 15 mm x 17 mm in the X and Y directions were used in the electrodiffusion experiments. Such samples are a convenient size for the sweeping apparatus and for subsequent infrared evaluation. Polished AT-cut rectangular plates and plano-convex AT-cut resonator blanks were swept for the mechanical and acoustic loss measurements, respectively.

Prior to sweeping, the samples were given an optical polish. Our sweeping process, which was carried out in the system previously described,[21] begins by vapor depositing gold electrodes on the two sample faces. If Li^+ or Na^+ is to be swept, the appropriate salt is first evaporated on one side, then a gold electrode is deposited over the salt. The electro-diffusion is carried out in the desired atmosphere at a temperature between 480^oC and 500^oC. Alkali sweeps (i.e., taking alkalis into the crystal) are done in a vacuum while an H_2 atmosphere is used for sweeping protons into the crystal. The applied electric field is approximately 15 V/cm for alkali sweeps

9

and 2000 V/cm for hydrogen. A digital multimeter and a laboratory computer are used to monitor the sweeping current as a function of time. Hydrogen sweeps are carried out until the current reaches a steady state; this usually takes less than 24 hours. Alkali sweeps continue until a sufficient number of ions have been transported; this usually takes less than two hours. As a sweep nears completion, we believe only one species of ion is being transported. Then, while the furnace temperature is slowly programmed down, the sample current is recorded as a function of temperature. This latter data gives the effective ionic conductivity as a function of temperature for the specific ion being swept.

Eight AT-cut polished rectangular plates approximately 15 mm x 20 mm x 2 mm thick were fabricated from each of the bars EG-C, PQ-C, TD-A, and PQ-D. Four plates from each of the bars EG-C, PQ-C, and TD-A were hydrogen-swept by the process described above. (Bar PQ-D was Sawyer-swept Premium Q grade material.) Two unswept and two swept plates from each of the bars were then etched in a concentrated ammonium bifluoride solution to reveal their etch tunnels. Except for PQ-D, each bar gave pairs of AT-cut plates representing each of the following four categories: unswept, unswept-etched, H-swept, and H-swept-etched. Samples for the X-parallel fracture tests were 1.5 mm wide with their long axis parallel to X and were cut from one plate of each pair. Z'-parallel fracture test samples, also 1.5 mm wide, were cut perpendicular to the X axis of the other member of each pair. The fracture stress was measured using a four point bend jig mounted in an Instron testing machine.[23] The four-point bend

test subjects the sample (at least in the elastic region) to a
pure bending moment between the inner loading points. The stress
varies from tension along the long axis of the sample on the top
to compression on the bottom. The results from at least seven
samples from each plate were averaged to obtain the values
reported.

Results and Discussion

The electrodiffusion current for the hydrogen sweeping
usually shows a significant initial decay followed by a steady
current as shown in Fig. 1 for sample PQ-G. The results for a
Li^+ sweep on a similar sample are also illustrated in Fig. 1.
Both the H^+ and Li^+ sweeps show nearly the same final current
even though the applied fields for the H^+ run is approximately
2000 V/cm while 15 V/cm was used for the Li^+ sweep. This result
and similar results for Na^+ show that H^+ is much less mobile than
alkali ions. We believe that the large initial current and
subsequent decrease that takes place in a H^+ sweep is caused by
the removal of the very mobile alkali ions from the sample.

Specific ions, Li^+ from the LiCl source electrode or H^+ from
the hydrogen atmosphere, are brought into the crystal at the
positive electrode. These specific ions then migrate along the Z
axis channel and replace the interstitial alkalis originally
trapped at the aluminum and similar sites. Thus, as the process
continues a condition is reached where only one species of ion is
migrating along the Z axis channel. The number of migrating ions

is determined by the number of traps present in the sample. Consequently, the conductivity should be described by Eqs. 1 through 5. Figure 2 shows a plot of $\log \sigma T$ versus $1000/T$ for Li^+, Na^+, and H^+ sweeps of previously unswept samples taken from bar HA-A. Bar HA-A, which was doped with aluminum during growth, contains very few OH^--related growth defects.[21] The apparent ionic conductivity of H^+ is seen to be much less than that of either Na^+ or Li^+. The upper half of Fig. 3 compares the apparent ionic conductivity of Li^+ in the HA-A sample, in Premium Q sample PQ-I (≈ 10 ppm Al), and in Super Premium Q sample SP-A (<1 ppm Al). The bottom half of Fig. 3 compares the conductivity of H^+ in sample HA-A and PQ-I. For both Li^+ and H^+ runs, the conductivity clearly increases with increasing Al content.

The activation energy, E, which includes both the migration energy and the association energy can be determined from the slope of the $\log \sigma T$ vs $1000/T$ curves. Table I gives the activation energies determined for Li^+, Na^+, and H^+ for a number of different sweeping runs. The activation energies vary considerably between the different quartz samples. The migration energy for a given ion is expected to be the same for all quartz, but different samples will have different traps so the association energy may fluctuate considerably. Bar SP-A is a very clean bar of quartz while both PQ-G and PQ-I have quite a bit of aluminum and other defects. Bar HA-A has a lot of aluminum but it is otherwise relatively defect free. Since the Al should dominate over other traps in bar HA-A, the activation energies reported for it may represent the effects of Al as the only trap. Our activation energies for the alkali ions are

12

Table I. Sweeping activation energies (in eV).

Sample	Li$^+$	Na$^+$	H$^+$
SP-A	0.76	0.99	1.75
PQ-G	1.14	1.25	1.95
PQ-I	0.98	1.13	1.93
HA-A	0.94	1.00	1.52
Literature	0.76-0.88[24]	1.03-1.2[24]	1.71-1.75[25]

slightly lower than the 1.3 to 1.4 eV found by Jain and Nowick[20] in their ionic conductivity studies.

Vig[17] has reported that sweeping lowers the etch tunnel density and improves the mechanical strength of quartz resonator blanks. We have carried out etching and four-point bend fracture tests on a number of unswept and H$^+$-swept synthetic quartz samples. Table II gives the etch tunnel density for unswept and H$^+$-swept samples from three bars of synthetic quartz.

Table II. Etch tunnel densities (tunnels/cm^2).

	EG-C	PQ-C	TD-A
Unswept	1300	1365	1710
H$^+$-swept	310	380	820

13

These results show that sweeping significantly reduces the etch tunnel density. However, the basic extended defect is still present. The sweeping has most likely replaced the alkali ions trapped in the dislocation network with protons.

Four-point bend fracture tests were made on samples cut parallel (X-parallel) and perpendicular (Z'-parallel) to the X axis of AT-cut synthetic quartz plates. Figure 4 shows the fracture stress results for unswept, unswept and etched, H^+-swept, and H^+-swept and etched X-parallel samples from Sawyer-swept bar PQ-D. Figure 5 shows the results for Z'-parallel samples. Our results as shown in Figure 4 and 5 indicate that swept and etched samples have the highest fracture strength. Etching alone might be expected to improve fracture resistance since it should improve the surface finish. However, the unswept-etched X-parallel samples showed a reduced strength while for Z'-parallel the unswept-etched samples were stronger.

Conclusions

The mobility of H^+ in the electrodiffusion process is much less than that of the alkali ions. As expected, the apparent ionic conductivity for a specific ion scales roughly with the aluminum content of the quartz. Since the activation energy for a specific ion depends upon the quality of the quartz, more than one type of trap must be involved. Hydrogen sweeping significantly reduces the formation of etch tunnels. Etched H^+-swept samples showed an improved fracture strength.

References

1. L. E. Halliburton, N. Koumvakalis, M. E. Markes, and J. J. Martin, J. Appl. Phys. 52, 3565 (1981).

2. D. R. Koehler and J. J. Martin, Proceedings of the 37th Annual Symposium on Frequency Control (1983).

3. D. B. Fraser, in Physical Acoustics, W. P. Mason, ed., Vol. V, pp. 54-110 (Academic Press, New York, 1968).

4. D. R. Koehler, Proceedings of the 35th Annual Symposium on Frequency Control (1981), p. 322.

5. H. G. Lipson, A. Kahan, R. N. Brown, and F. K. Euler, Proceedings of the 35th Annual Symposium on Frequency Control (1981), p. 329.

6. J. C. King, Bell System Tech. J. 38, 583 (1959).

7. A. Kats, Philips Res. Repts. 17, 133 (1962).

8. D. B. Fraser, J. Appl. Phys. 35, 2913 (1964).

9. G. B. Krefft, Rad. Effects 26, 249 (1975).

10. R. N. Brown, J. O'Connor, and A. F. Armington, Mat. Res. Bull. 15, 1063 (1980).

11. T. M. Flanagan and T. F. Wrobel, IEEE Trans. Nucl. Sci. NS-16, 130, (Dec. 1969).

12. J. C. King and H. H. Sanders, IEEE Trans. Nucl. Sci. NS-19, 23 (1972).

13. P. Pelligrini, F. Euler, A. Kahan, T. M. Flanagan, and T. F. Wrobel, IEEE Trans. Nucl. Sci. NS-25, 1267 (1978).

14. G. W. Arnold, Proceedings of the 11th Annual Symposium on Frequency Control (1957), p. 119.

15. J. W. Nielson and F. G. Foster, Am. Mineral. 45, 299 (1960).

16. W. J. Spencer and K. Haruta, J. Appl. Phys. 35, 2368 (1964).

17. J. R. Vig, J. W. LeBus, and R. L. Filler, Proceedings of the 31st Annual Symposium on Frequency Control (1977), p. 131.

18. A. D. Franklin, in Point Defects in Solids, J. H. Crawford and L. M. Slifkin, eds., (Plenum, New York, 1972), Vol. 1, Chap. 1.

19. A. B. Lidiard, Handbuch der Physik 20, 246 (1957).

20. H. Jain and A. S. Nowick, J. Appl. Phys. 53, 477 (1982).

21. J. J. Martin, L. E. Halliburton, R. B. Bossoli, and A. F. Armington, Proceedings of the 36th Annual Symposium on Frequency Control (1982), p. 77.

22. M. E. Markes and L. E. Halliburton, J. Appl. Phys. 50, 8172 (1979).

23. W. A. Sibley, C. T. Butler, J. R. Hopkins, J. J. Martin, and J. A. Miller, Growth and Hardening of Alkali Halides for Use in Infrared Laser Windows, Technical Report, AFCRL-TR-0342 (1973).

24. J. Verhoogen, Am. Mineral. 37, 637 (1952).

25. H. Wendon, Am. Mineral. 42, 859 (1957).

Figure Captions

1. The electrodiffusion currents for H^+ and Li^+ sweeps on samples from Sawyer Premium Q bar PQ-G are shown as functions of time. We believe that the large initial decay during a H^+ sweep is caused by the replacement of the mobile alkalis with protons. The applied fields were 2000 V/cm for H^+ and 15 V/cm for Li^+.

2. The product of the apparent ionic conductivity times the temperature in samples taken from the aluminum-doped quartz bar HA-A. In all cases the conductivity is thermally activated.

3. The upper portion of the graph compares σT vs 1000/T for Li^+-swept samples with approximately 50 ppm Al (HA-A), 10 ppm Al (PQ-I), and less than 1 ppm Al (SP-A). The lower portion compares σT vs 1000/T for samples with approximately 50 and 10 ppm Al.

4. The fracture stress as measured under four-point bend is shown for test sample bars cut from AT-plates parallel to the X axis. I corresponds to as-received material while II corresponds to H^+-swept (E indicates etched). The samples are A (Sawyer EG-C), B (Sawyer PQ-C), C (Thermodynamics TD-A), and D (Sawyer-swept PQ-D). Etched H^+-swept samples show a higher fracture strength.

5. The fracture stress as measured under four-point bend is shown for test sample bars cut from AT-plates perpendicular to the X axis. The sample designations are the same as in Fig. 4.
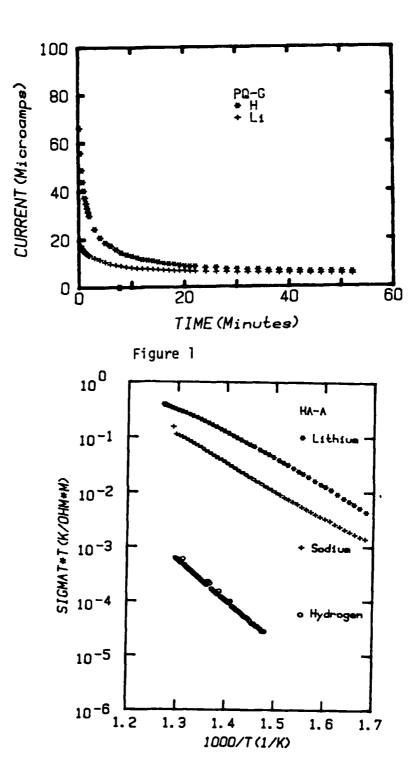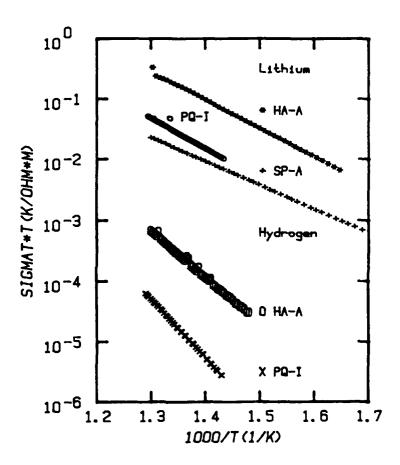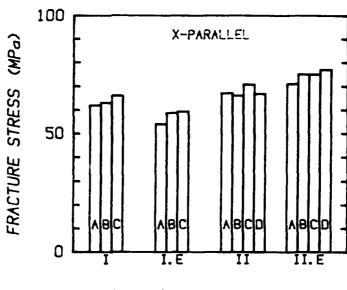
Figure 1

Figure 2

18

Figure 3

19

Figure 4

Figure 5

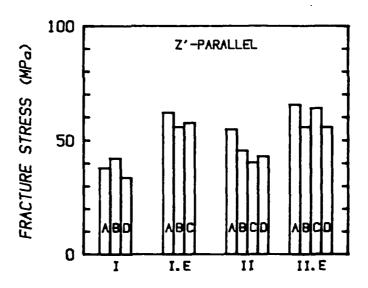# III.   ALUMINUM-RELATED ACOUSTIC LOSS IN AT-CUT QUARTZ CRYSTALS

Introduction

Alpha-quartz is used in a wide variety of precision
electronic devices where aging and radiation-induced instabil-
ities are undesirable. It is now well-known that quartz-
controlled oscillators may exhibit transient and steady-state
frequency and Q shifts when exposed to ionizing radiation.[1-3]
Early results obtained by King[4] and other investigators[5-8]
suggested that these effects were associated with the presence of
impurities.

Substitutional Al^{3+} is present in all quartz[9] and requires
charge compensation. Examples of such charge compensators are
interstitital Li^+ or Na^+ ions, or holes or protons at an oxygen
ion adjacent to the aluminum. The proton forms an OH^-
molecule which is infrared active.[9,10] The $Al-Na^+$ defect is
responsible for the acoustic loss peak observed near 53 K in 5 MHz
5th overtone AT-cut crystals.[11] Irradiation at room temperature
destroys the $Al-Na^+$ centers,[4,12] and this is responsible for much
of the steady-state frequency offset. Recent work at Oklahoma
State University has shown that the alkali ions become mobile
under irradiation only if the temperature is greater than 200
K.[12-14] Following a room-temperature irradiation, either a hole
which can be observed by ESR techniques or a proton is found
trapped on an oxygen adjacent to the Al^{3+}. The interstitial
alkali ions are usually in the relatively large Z-axis channels
and at high temperatures can move along the channel under an

applied electric field. King,[4] and later Kats[10] and Fraser,[11] used this technique to "sweep" hydrogen and specific alkalis into the sample. Sweeping hydrogen in to replace the alkalis has been shown to improve the radiation hardness of quartz oscillators.[7]

The identification of both growth and radiation-induced defects which affect the performance of quartz resonators is an important part of our project. Recently, using sweeping, IR absorption, and acoustic loss measurements, Martin and Doherty[15] reported that the Al-OH⁻ center does not have an acoustic loss peak at temperatures below 370 K. They also reported that irradiation of both unswept and H_2-swept Premium Q quartz resonator blanks produced acoustic loss peaks at 23 K and 100 K and a broad loss peak between 125 K and 165 K. King and Sander[1] had earlier reported the two higher temperature peaks and had suggested that they were caused by the Al-hole center. The 23 K peak had also been observed earlier and was attributed to changes in the interaction between the resonant vibrations of the blank and the thermal phonons.[16] We report here a comparison of the acoustic loss spectra of as-received, Li^+, Na^+, and H^+-swept resonators fabricated from the same bar of Premium Q grade quartz. We also report an isochronal anneal study of the three peaks induced by a room-temperature irradiation which shows that they are associated with the Al-hole center. An isochronal anneal study was also made on an irradiated Na^+-swept resonator to directly compare the decay of the Al-hole center and Al-OH⁻ center with the recovery of the $Al-Na^+$ center.

22

Experimental Procedure

Most samples for this study were cut from an unswept pure z-growth Sawyer Premium Q bar of cultured quartz that has been given an in-house designation PQ-E. Samples from this bar have been extensively studied at Oklahoma State University using ESR, IR, and acoustic loss techniques. All of these investigations show that the bar is of high quality but that it contains somewhat more aluminum (10-15 ppm) than the average Premium Q material (5-8 ppm). Consequently, aluminum-related effects are more readily observed. Confirming measurements were made on samples from Toyo Supreme Q bar SQ-B.

Five MHz 5th overtone AT-cut plano convex resonator blanks of the Warner design[17] were fabricated for this study by K&W Mfg., Prague, OK. The acoustic loss, Q^{-1}, of the resonator blanks was measured by the log decrement method from 5 to 300 K. The measurements were made in a variable temperature helium Dewar with the blanks mounted in a gap holder similar to the one described by Fraser.[16] The blank was driven for 10 ms at its series resonant frequency and then allowed to freely decay. The decaying rf signal was detected with a superheterodyne detector and displayed on a variable persistance storage oscilloscope. The exponential decay times were measured using a window detector to gate a digital timer.

Electrolysis, or sweeping, was carried out at temperatures of 470-480°C in a controlled-atmosphere system. This system allowed the use of H_2, D_2, or gettered-N_2 atmospheres, or an oil-diffusion pumped vacuum of approximately 2×10^{-6} Torr. For the

acoustic loss studies, the AT-cut resonator blanks were directly swept. Vapor-deposited Au electrodes were used. For the Li or Na sweeping runs, LiCl or NaCl was vapor deposited on the sample surface and then a Au electrode was deposited over the salt layer. The Li and Na sweeps were carried out in a vacuum better than 5×10^{-6} Torr. Infrared absorption scans show that Al-OH$^-$ centers are present in the H_2-swept sample but not in the alkali-swept samples.

Irradiations were carried out at room temperature using 1.7-MeV electrons from a Van de Graaff accelerator. Typical doses were approximately 2000 J/cm^3 ($\approx 10^8$ rads). This dose is not expected to produce significant knock-on damage, but it has been shown to saturate the Al-related defects. The production of Al-OH$^-$ centers by the irradiation was measured by a liquid nitrogen temperature polarized infrared scan on the resonator blank. Isochronal anneals were carried out with the blank in the bottom half of the gap holder. A hole in the side of the holder was used to determine the sample temperature. The sample was held "at temperature" for five minutes, then removed from the furnace and re-installed in the cyrostat after "air cooling" to room temperature.

Results and Discussion

Figure 1 compares the acoustic loss, Q^{-1}, spectra for unswept, Li-swept, and Na-swept PQ-E series resonator blanks. The unswept blank shows a small Al-Na$^+$ loss peak at 53 K with a height ΔQ^{-1} of approximately 0.5×10^{-6}. The Li sweep removed

24

this peak and did not introduce any new peaks. The Na-swept
blank showed a very large 53 K with $\Delta Q^{-1} = 2 \times 10^{-4}$, as shown in
Fig. 1. Since the material from which these blanks were
fabricated contains 10 to 15 ppm aluminum, we conclude that the
concentration, C, of Al-Na$^+$ centers is given by

$$C = [5 \ (\pm 20\%) \times 10^4] \ \Delta Q^{-1} \tag{1}$$

where C is in ppm and ΔQ^{-1} is the height of the 53-K Al-Na$^+$ loss
peak. Thus, the unswept PQ-E blank probably contains about 0.3
ppm Al-Na$^+$ centers; the remaining 10 to 15 ppm of aluminum must
be compensated by Li$^+$. Since the mineralizer used in growing
Premium Q quartz is predominantly $NaCO_3$, the essentially total
exclusion of Na$^+$ from the aluminum sites by the addition of a
small amount of $LiCO_3$ to the solution is remarkable.[18] Since
both the unswept and Li-swept blanks must contain 10-15 ppm Al-
Li$^+$ centers, we believe that the Al-Li$^+$ center does not couple to
the AT-cut thickness-shear mode. An additional, much smaller,
loss peak related to the Al-Na$^+$ center was observed at
approximately 135 K in the Na-swept blank. Park and Nowick[19]
have also observed two Na-related peaks in their dielectric loss
measurements.

Figure 2 compares the acoustic loss spectra for the unswept,
Li-swept, and H-swept blanks. The results for the lithium and
hydrogen sweeps are essentially identical, as were the results
from a deuterium sweep which were omitted from Fig. 2 for
clarity. Infrared absorption measurements made at liquid

25

nitrogen temperature show that the H^+-swept blank contains 10-15 ppm Al-OH⁻ centers. Thus, it appears that neither the Al-OH⁻ or the Al-OD⁻ centers show significant acoustic loss peaks at temperatures below about 370 K. It should be noted that at higher temperatures, the interstitial alkali ions become thermally liberated from the Al^{3+} trapping site and diffuse along the Z-axis channels. This diffusion causes an acoustic loss which increases exponentially with temperature.[16] Lipson et al.[20] and Koehler[21] have shown that this high temperature loss is not present in H^+-swept quartz which contains no alkali ions, and therefore, must be caused by the alkali diffusion.

Recently, Martin and Doherty[15] reported that irradiation of unswept and H^+-swept PQ-E resonator blanks at room temperature produced loss peaks at 23 K and 100 K and a broad loss between 125 and 165 K. The peaks were much larger in the unswept material than in the H^+-swept blank. The room-temperature irradiation also removed the $Al-Na^+$ loss peak which was present initially in the unswept blank. King and Sander[1] have previously observed the peak at 100 K and the broad loss between 125 K and 165 K. They attributed these loss peaks to the Al-hole center. Martin and Doherty suggested that the 23 K peak is also due to the Al-hole center. Martin et al.[22] were able to describe the broad loss as a single peak centered at about 135 K.

Figure 3 shows the acoustic loss, Q^{-1}, versus temperature spectrum for the Na-swept blank in the as-swept condition and after a room-temperature irradiation. The irradiation has removed the large 53 K and 135 K $Al-Na^+$ loss peak while introducing the 23 K, 100 K, and 135 K peaks. The post-

26

irradiation acoustic loss spectra for the unswept and Li-swept blanks are essentially the same as for the Na-swept sample. These three loss peaks are also observed in irradiated H^+-swept resonators fabricated from this same bar. However, their strength is reduced by approximately a factor of five. An inspection of the results reported by Doherty et al.[12] for the acoustic loss of their Na-swept resonator D14-45DC shows that the 25 K peak is small but present in their results. D14-45 series quartz has an aluminum content less than 1 ppm, so we would expect aluminum-related loss peaks to be much smaller Their Na loss peak is about 0.035 times that in our Na-swept PQ-E resonator blank. It should also be noted that their resonator was partially H^+-swept. Thus, it appears that these three peaks, and the Na peak as well, scale with the aluminum content.

The thermal anneal behavior of the Al-hole and $Al-OH^-$ centers in unswept quartz has been studied by Markes and Halliburton[13] and by Sibley et al.,[14] respectively. The Al-hole centers, as observed by ESR techniques, anneal out slightly below 550 K while the $Al-OH^-$ center anneals out between 620 K and 670 K. If the three radiation-induced loss peaks are due to the Al-hole center, they should show the same annealing pattern as the Al-hole center ESR spectrum. We have carried out an isochronal anneal study on the unswept blank and on the Li-swept blank. The results for the unswept blank show that the 25 K, 100 K, and 135 K loss peaks all anneal out between 500 and 550 K, as shown in Fig. 4. Thus, all three loss peaks are most likely caused by the Al-hole center. When the anneal of the unswept blank is

continued to higher temperatures, the Al-Na$^+$ center loss peak recovers between 600 and 650 K as shown in Fig. 4.

The isochronal anneal study also showed that after a room temperature irradiation and subsequent 670 K anneal, the 53 K Al-Na$^+$ peak in the unswept blank increased by approximately a factor of four (from 0.5 x 10^{-6} to 2.2 x 10^{-6}). The Al-Na$^+$ loss peak also appeared in the Li-swept sample as a result of annealing although it was absent in the as-Li-swept sample. These latter results suggest that Na is trapped at sites other than aluminum during growth. The irradiation and anneal treatment just described evidently rearranged the alkalis within the sample. It is conceivable that this process would take place at the 50 to 80°C operating temperature of a crystal oscillator (although very slowly) and contribute to the long term aging of the crystal.

The decay of the radiation-induced Al-hole center should be matched by the corresponding growth of the Al-OH$^-$ and/or Al-M$^+$ centers. Sibley et al.[14] have measured the high temperature annealing behavior of the radiation-induced Al-OH$^-$ center. Their results do not show any changes in the Al-OH$^-$ concentration for the 500-550 K temperature range where the Al-hole center decays. This result suggests that the anneal of the Al-hole center is matched by the return of an alkali ion to the Al site. Since both our unswept samples contain mostly Li$^+$ ions and the Al-Li$^+$ center does not have an acoustic loss peak, Fig. 4 does not show the expected return of the alkali ions. We have repeated the isochronal anneal study using the Na-swept blank. In this investigation acoustic loss measurements of the 23 K Al-hole peak and 53 K Al-Na$^+$ peak were used to track the behavior of the hole

and alkali centers. Polarized infrared absorption measurements of the 3367 cm^{-1} band were also made on the Na-swept blank in order to track the Al-OH$^-$ center. Figure 5 shows that the decay of the 23 K Al-hole center acoustic loss peak in the 500 K to 550 K range is matched by an approximately 25% growth in the 53 K Al-Na$^+$ acoustic loss peak. The remaining recovery of the Al-Na$^+$ center closely matches the decay of Al-OH$^-$ centers as measured by infrared absorption. The increase in the Al-OH$^-$ center observed near 350 K does not have a corresponding change in either the Al-hole center or Al-Na$^+$ center. The annealing results shown in Fig. 5 suggest that the room temperature irradiation converted approximately 25% of the Al sites into Al-hole centers with the remaining 75% becoming Al-OH$^-$ centers. In this process, the Na$^+$ leaves the Al site and is subsequently trapped at as yet unknown sites in the crystal. Figure 6 shows the results plotted on this normalized basis. When the Al-hole center anneals out in the 500 to 550 K temperature range the Na$^+$ ion returns to the Al site. In unswept material the decay of the Al-hole center must be accompanied by the return of a Li$^+$ ion since no corresponding increase in the Al-OH$^-$ center is seen.

Often defect-related acoustic loss peaks can be described by

$$\Delta Q^{-1} = \frac{D \omega \tau}{1 + \omega^2 \tau^2} \tag{2}$$

where ΔQ^{-1} is the loss above the intrinsic background, D is the strength factor, ω is the angular frequency, and τ is the relaxation time for reorientation of the defect. The relaxation

29

is usually thermally activated as the defect must go over an energy barrier to reach the equivalent sites.[16] Thus,

$$\tau = \tau_o \exp(E/kT) \qquad (3)$$

where E is the barrier height and τ_o contains the number of equivalent orientations and the attack rate. We have fit Eq. 1, with the relaxation time given by Eq. 3, to the 53 K and 135 K Al-Na$^+$ center loss peaks and to the three radiation-induced Al-h$^+$ peaks. The calculated parameters are given in Table I. Our activation energies and relaxation times for the Al-Na$^+$ center are in good agreement with Park and Nowick's dielectric loss results,[19] as well as those of Stevels and Volger.[23]

Stevels and Volger have also reported a radiation-induced dielectric loss peak with E = 7.5 meV and τ_o = 5 x 10^{-7} sec. This activation energy is in reasonable agreement with our 23 K

Table I. Loss peak parameters.

T(K)	E(meV)	τ_o(sec)	Defect
53	57	1.65 x 10^{-13}	Al-Na$^+$
135	130	4.44 x 10^{-13}	Al-Na$^+$
23	8	8.3 x 10^{-10}	Al-hole
100	9	1.0 x 10^{-12}	Al-hole
135	110	2.7 x 10^{-12}	Al-hole

peak, but the relaxation time is much longer. Taylor and Farnell[24] have also made dielectric loss measurements on irradiated quartz; they found a loss peak near E = 7.5 meV, in agreement with Stevels and Volger, and an additional peak at low temperature with E = 1.2 meV and τ_0 = 6.2 x 10^{-5} sec.

Conclusions

Sweeping Li^+, H^+, or D^+ into high-aluminum-content Premium Q grade quartz AT-cut resonators removes the small $Al-Na^+$ loss peak at 53 K but does not introduce any new loss peaks at temperatures below 370 K. Therefore, we conclude that the $Al-Li^+$ and $Al-OH^-$ centers do not couple to the AT thickness shear mode. Na-swept samples show a very large 53 K loss peak. This shows that in as-grown quartz most of the Al sites are compensated by Li^+. Irradiation at room temperature replaces the interstitial alkali at the Al sites with a mixture of Al-hole and $Al-OH^-$ centers. These radiation-induced Al-hole centers are responsible for acoustic loss peaks at 23 K, 100 K and 135 K. The annealing of the Al-hole centers between 500 and 550 K is matched by a corresponding return of the alkali ions to the Al sites. The higher temperature decay of the $Al-OH^-$ center is also matched by the growth of the $Al-M^+$ centers.

References

1. J. C. King and H. H. Sander. IEEE Trans. Nucl. Sci. NS-19, 23 (1972).

2. P. Pelligrini, F. Euler, A. Kahan, T. M. Flanagan, and T. F. Wrobel, IEEE Trans. Nucl. Sci. NS-25, 1267 (1978).

3. T. J. Young, D. R. Koehler, and R. A. Adams, Proceedings of the 32nd Annual Symposium on Frequency Control (1978), p. 34.

4. J. C. King, Bell System Tech. J. 38, 573 (1959).

5. R. A. Poll and S. L. Ridgway, IEEE Trans. Nucl. Sci. NS-13, 130 (December, 1966).

6. T. M. Flanagan and T. F. Wrobel, IEEE Trans. Nucl. Sci.NS-16, 130 (December, 1969).

7. B. R. Capone, A. Kahan, R. N. Brown, and J. R. Buckmelter, IEEE Trans. Nucl. Sci. NS-17, 217 (December, 1970).

8. T. M. Flanagan, IEEE Trans. Nucl. Sci. NS-21, 390 (December, 1974).

9. L. E. Halliburton, N. Koumvakalis, M. E. Markes, and J. J. Martin, J. Appl. Phys. 52, 3565 (1981).

10. A. Kats, Philips Res. Repts. 17, 133 (1962).

11. D. B. Fraser, J. Appl. Phys. 35, 2913 (1964).

12. S. P. Doherty, J. J. Martin, A. F. Armington, and R. N Brown, J. Appl. Phys. 51, 4164 (1980).

13. M. E. Markes and L. E. Halliburton, J. Appl. Phys. 50, 8172 (1979).

14. W. A. Sibley, J. J. Martin, M. C. Wintersgill, and J. D. Brown, J. Appl. Phys. 50, 5449 (1979).

15. J. J. Martin and S. P. Doherty, Proceedings of the 34th Annual Symposium on Frequency Control (1980), p. 81.

16. D. B. Fraser, Physical Acoustics, W. P. Mason, ed. (Academic Press, New York, 1968) Vol. V, Chap. 2.

17. A. W. Warner, Bell System Tech. J. 40, 1193 (1960).

18. J. C. King, A. A. Ballman, and R. A. Laudise, J. Phys. Chem. Solids 23, 1019 (1962).

19. D. S. Park and A. S. Nowick, Phys. Stat. Sol. (a) 26, 617 (1979).

20. H. G. Lipson, A. Kahan, R. N. Brown, and F. Euler, Proceedings of the 35th Annual Symposium on Frequency Control (1981), p. 329.

21. D. R. Koehler, Proceedings of the 35th Annual Symposium on Frequency Control (1981), p. 327.

22. J. J. Martin, L. E. Halliburton, and R. B. Bossoli, Proceedings of the 35th Annual Symposium on Frequency Control (1981), p. 317.

23. J. M. Stevels and J. Volger, Philips Res. Repts. 17, 284 (1962).

24. A. L. Taylor and G. W. Farnell, Can. J. Phys. 42, 595 (1964).

Figure Captions

1. The acoustic loss versus temperature spectra for unswept, Li-swept, and Na-swept blanks taken from Sawyer Premium Q bar PQ-E are shown. These results show that in unswept Premium Q material Li^+ is the dominant alkali ion at the Al site.

2. The acoustic loss versus temperature spectra for unswept, Li-swept, and H-swept blanks taken from Sawyer Premium Q bar PQ-E are shown. No loss peaks attributable to either the $Al-Li^+$ or $Al-OH^-$ center are observed.

3. The acoustic loss versus temperature spectra taken on the Na-swept blank are shown before and after a room-temperature irradiation. The irradiation has removed the 53-K and 135-K $Al-Na^+$ loss peaks and produced new peaks at 23, 100, and 135 K. A similar irradiation of the unswept and Li-swept blanks produced identical spectra.

4. The radiation-induced 23, 100, and 135 K loss peaks in the unswept sample anneal out together between 500 and 550 K. This behavior matches the decay of the Al-hole center. The 53-K $Al-Na^+$ center recovers at higher temperatures.

5. The annealing of the radiation-induced Al-hole and $Al-OH^-$ centers and the recovery of the $Al-Na^+$ centers are shown for the Na-swept sample. The decay of the Al-hole center is matched by the return of approximately 25% of the $Al-Na^+$ centers.

6. The annealing behavior of the Al-hole and $Al-OH^-$ centers normalized to the total Al is shown.
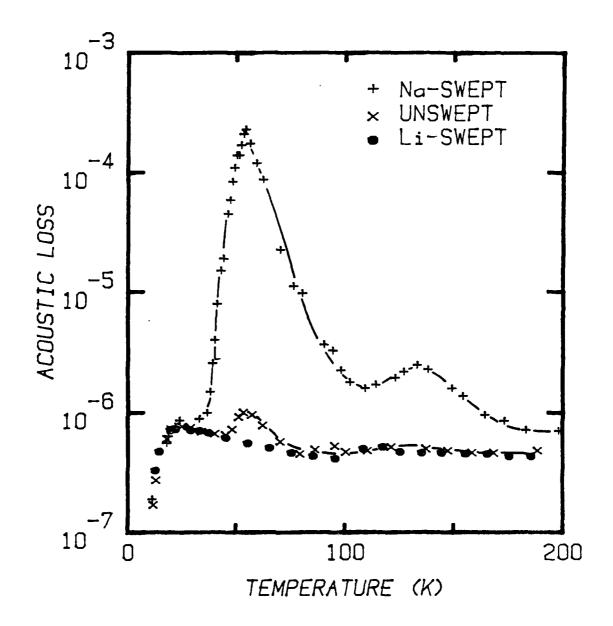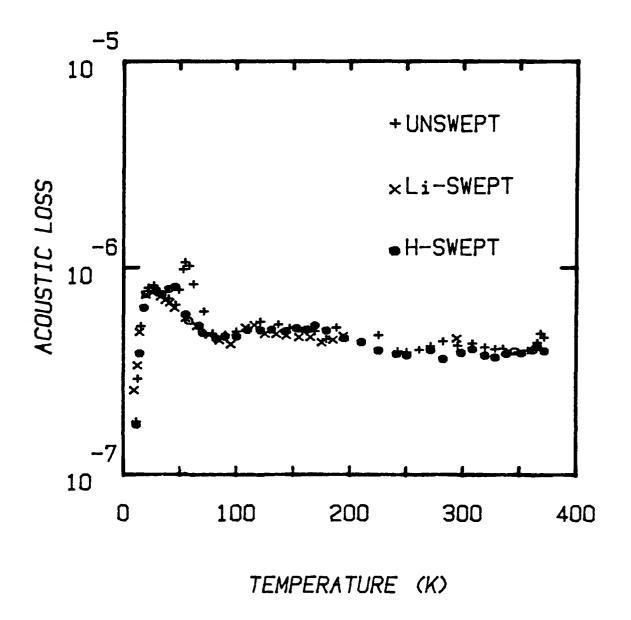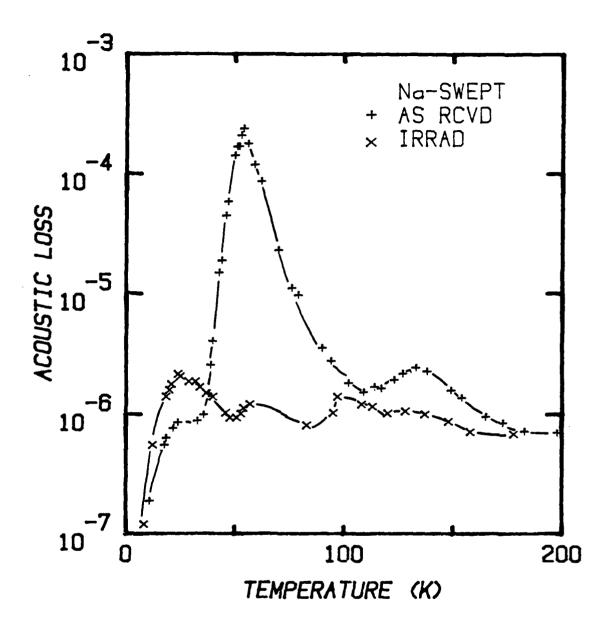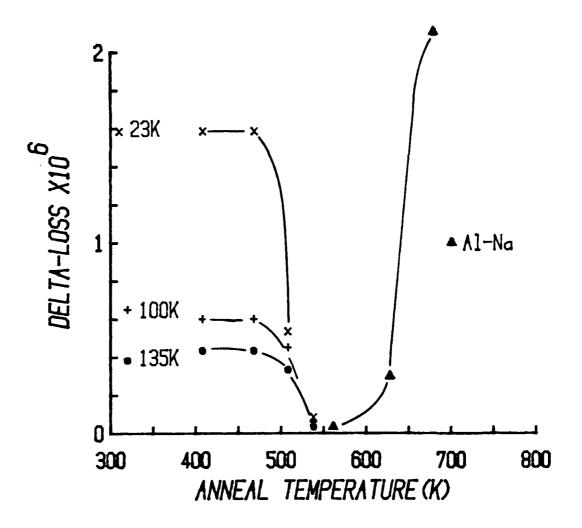
34
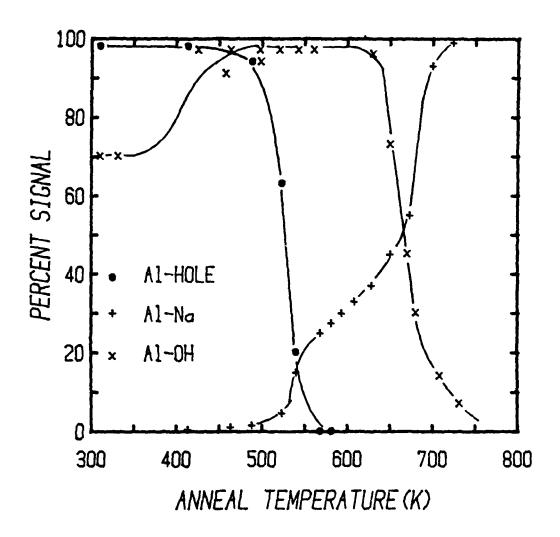
Figure 1
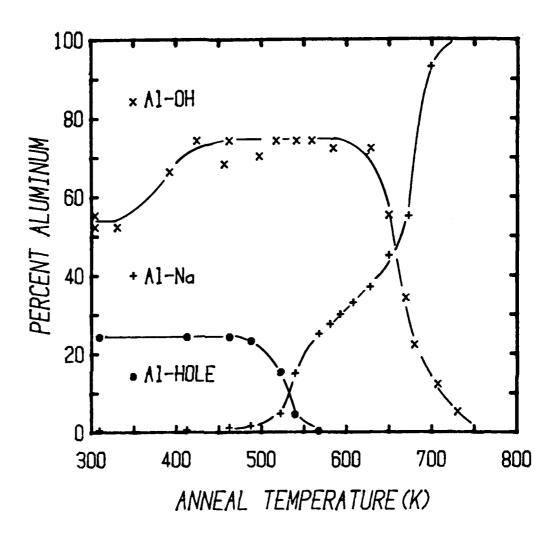
Figure 2

36

Figure 3

Figure 4

Figure 5

39

Figure 6

40

IV. ^{27}Al HYPERFINE AND QUADRUPOLE INTERACTIONS FOR THE [AlO$_4$]^0 CENTER IN QUARTZ

Introduction

The "aluminum-hole" center, more precisely referred to as the [AlO$_4$]^0 center, is formed in aluminum-containing quartz by irradiation with high-energy photons or particles. This defect is best known as the origin of the familiar smoky coloration in quartz,[1] and it also plays an important role in the radiation response of the material.[2] In 1955, Griffiths et al.[3] described the initial electron spin resonance (ESR) study of the [AlO$_4$]^0 center. Since then, many studies of this and similar centers have been reported.[4-13] The recent review by Weil[8] and the papers by Nuttall and Weil[11-13] give an excellent introduction to the literature on the aluminum-associated trapped-hole centers in quartz.

O'Brien[4] proposed a model for the [AlO$_4$]^0 center which consisted of a hole localized in a non-bonding oxygen 2p (π-type) orbital adjacent to the substitutional aluminum ion. This basic model has survived the numerous later studies of the center and is generally accepted today. In their recent contribution, Nuttall and Weil[11] have greatly extended our knowledge of the [AlO$_4$]^0 center by carefully measuring the g matrix, the ^{27}Al hyperfine and quadrupole matrix, the ^{17}O hyperfine matrix, and the ^{29}Si hyperfine matrix. They were able to determine the nuclear quadrupole parameters because the [AlO$_4$]^0 center ESR spectrum, taken at 9 GHz, contains many "forbidden" lines.

An ENDOR study by Barker[9] gave values for the ^{27}Al hyperfine and quadrupole matrices, but these results were limited by several factors including a lack of precision in orienting the sample.[11] Since ENDOR experiments provide greater resolution than ESR experiments, we believed it worthwhile to repeat and extend the ENDOR work of Barker and provide direct verification of the ^{27}Al hyperfine and quadrupole parameters presented by Nuttall and Weil.[11] Also, we have analysed the anisotropic portion of the ^{27}Al hyperfine in terms of contributions from both simple dipole-dipole effects and unpaired spin density in the 3p orbitals of the aluminum impurity ion. Our calculations extend the earlier results of Nuttall and Weil where they found that this anisotropic hyperfine could not be readily explained by only dipole-dipole calculations which took into account the spatial extent of the unpaired spin in the oxygen orbital.

Experimental

The sample of right hand quartz used in our ENDOR study was cut from the z-growth region of a bar of "Premium Q" material provided by Sawyer Research Products, Eastlake, Ohio. Sample size was 10 x 3.5 x 2 mm^3 in the X, Y, and Z directions, respectively. The direction of the +X axis (parallel to $+\vec{a}_1$) was determined by a "squeeze test", where the positive end of the X axis develops a negative charge during compression.[14] The [AlO$_4$]^0 centers were produced by room-temperature irradiation with 1.7 MeV electrons from a Van de Graaff accelerator.

The ENDOR experiment was done using a modified homodyne ESR spectrometer operating at X band. The microwave bridge contained a detector bias arm and a solid state microwave amplifier (Narda N6244S-37). A Varian 9-inch magnet with Fieldial regulation was used, and a Varian large access cylindrical cavity (E-235) was employed along with an Air Products Model LTD-3-110 variable temperature helium flow system. An ESR signal was obtained by modulating the magnetic field at 50 kHz and detecting with a PAR Model 128 lock-in amplifier. A Varian E-500 gaussmeter and an HP-5340A counter were used to measure the magnetic field and microwave frequency.

The ENDOR signal was acquired by monitoring the change induced in the ESR signal as the rf was rapidly swept across the frequency range of interest (2 to 18 MHz). An HP-8601A sweep generator and 10 W power amplifier provided the rf to a three-turn coil placed inside the microwave cavity. The frequency of the sweep generator was controlled by a Nicolet 1073 signal averager, which also accumulated the ENDOR spectrum. Typically, 500 sweeps, at a rate of approximately 5 to 10 sweeps/sec, were used to obtain a single ENDOR spectrum. The rf coil and the sample were mounted on separate dielectric forms which were placed in the cold helium gas flow within the cavity. This allowed rotation of the sample during the angular studies without moving the ENDOR coil relative to the cavity.

Results

The ENDOR spectrum shown in Fig. 1 is typical of our data obtained from the $[AlO_4]^{\circ}$ center in quartz. This particular spectrum was taken with the magnetic field parallel to the c axis and with a sample temperature of 20 K. Because the ^{27}Al hyperfine lines are well resolved in the ESR spectrum, only four ENDOR transitions are present in Fig. 1. Ten ENDOR lines are expected for a specific defect site because of the S = 1/2, I = 5/2 nature of the spin system. To observe the remaining six ENDOR lines not found in Fig. 1, it is necessary to take data at other ESR lines within the given hyperfine pattern.

As the magnetic field is rotated in the X plane of the sample, the $[AlO_4]^{\circ}$ centers separate into three magnetically inequivalent sites, which is reflected in the ESR spectrum by three sets of ^{27}Al hyperfine lines. We obtained ENDOR data from each of the three sites at six magnetic field directions (0°, 30°, 70°, 90°, 110°, and 150° relative to the c axis). The following spin-Hamiltonian was used to analyze the aluminum ENDOR data.

$$\mathcal{H} = \vec{S}\cdot\overleftrightarrow{g}\cdot\vec{H} + \vec{I}\cdot\overleftrightarrow{A}\cdot\vec{S} + \vec{I}\cdot\overleftrightarrow{Q}\cdot\vec{I} - g_N\beta_N\vec{I}\cdot\vec{H}$$

A total of 86 experimental ENDOR frequencies, with corresponding magnetic field values and microwave frequencies, were used as input data for a computer program which determined the principal values and angles of the aluminum hyperfine and quadrupole matrices. The g matrix given by Nuttall and Weil[11] and a value

44

of 0.0011094 MHz/G for $g_N\beta_N$ were used in the calculations.
Results of this "fitting" are given in Table I along with those
obtained by Nuttall and Weil[11] and by Barker.[9] The root-mean-
square deviation for our ENDOR line positions was 0.029 MHz.

Figure 2 illustrates the aluminum ion and surrounding oxygen
ions, with the equivalent atomic position coordinates given in
Table III of Reference 15 (NOTE: Si(0) must be replaced by
Al(0)). Our parameters in Table I correspond to having the hole
on O(3).

Discussion

As indicated in the introduction, a series of excellent
studies have provided adequate explanations of many of the
interesting properties of the $[AlO_4]^0$ center. However, one
feature which has not been explained by the earlier investigators
is the small magnitude of the anisotropic ^{27}Al hyperfine
interaction. To obtain agreement with experiment, a simple point
dipole-dipole calculation requires that the distance from the Al
nucleus to the oxygen on which the hole is trapped be increased
from 1.6 Å (the Si-O bond length) to near 2.3 Å.[16] Such a result
is clearly unreasonable. Barker[9] suggested that the distortion
would not have to be as large if negative unpaired spin density
were added at the aluminum.

Nuttall and Weil[11] considered the principal directions of
the aluminum and nearest-neighbor silicon hyperfine matrices as
an estimate of the oxygen's position. They found a reasonable
value for the displacement of the oxygen (0.27 Å from the normal

position) but this led to unreasonable (i.e., very small) spin

densities on the oxygen ion. They also approximated the hole

wavefunction as a grid of points and weighted the interactions of

these point dipoles with the ^{27}Al nuclear moment. Their

calculations included taking different forms of the oxygen

orbital by adding s contributions and by changing positions of

its axes and the position of the nucleus, but they still found

principal values for the anisotropic aluminum hyperfine which

were too large by factors of approximately three. In their

analysis of the ^{17}O hyperfine principal values of the $[AlO_4]^O$

center, Nuttall and Weil[11] estimated the total spin density on

the principal oxygen to be 0.77. The remaining spin density is

located at the neighboring aluminum, silicon, and oxygen ions.

To explain the anisotropic ^{27}Al hyperfine interaction, we

have taken into account unpaired spin density in aluminum 3p-type

orbitals in addition to the main dipole-dipole contribution with

the trapped hole's unpaired spin on the oxygen. We assumed the

aluminum 3p orbitals to be sp^3 types participating in σ-type

bonds with the surrounding oxygen ligand ions. Their

orientations, and hence the principal directions of their

contributions to the anisotropic hyperfine interaction, will be

along the bond directions to the oxygens surrounding the aluminum

impurity. The dipole-dipole interaction of the aluminum nucleus

with unpaired spin on these oxygen ligands will also have the

same principal directions along the bonds, and these two

contributions could not be separated in our simple approach.

The variation of the hyperfine splitting for rotation of the

magnetic field in the X plane was generated using the principal components of the experimental hyperfine matrix A and ignoring effects due to nuclear Zeeman, quadrupole, and second-order effects from the g shifts. These results are shown in Fig. 3 for each of the three inequivalent silicon sites. With this as data, a fitting program was constructed which varied the admixture of aluminum 3p-type orbitals (directed toward O(1), O(2), and O(4) in Fig. 2) and the magnitude of the main dipole-dipole interaction with the hole located on O(3). The results of this fit are given in Table II, and the corresponding "theoretical" hyperfine values are plotted as filled circles in Fig. 3. This shows that very good agreement with experiment is obtained by including the additional contributions to the hyperfine from these aluminum orbitals.

The magnitude of the dipole-dipole interaction obtained from our fit can be used to obtain an estimate of the aluminum-hole separation. For this purpose, we use the expression provided by Schirmer,[16] which includes an approximation for the spatial extent of the p-orbital on O(3), and the value of 0.77 as the spin-density associated with O(3).

$$A_{d-d} = (0.77) \, g_e \, g_N \, \beta \, \beta_N \left\{ \frac{1}{R^3} - \left(\frac{6}{5} \right) \frac{\langle \rho^2 \rangle}{R^5} \right\}$$

The mean square distance between the hole and oxygen nucleus, $\langle \rho^2 \rangle$, was taken to be 0.85 $\overset{\circ}{A}{}^2$. Our value of 1.70 MHz for the magnitude of the dipole-dipole interaction, A_{d-d}, results in a value of 1.88 $\overset{\circ}{A}$ for the Al-O(3) separation. This is only a 14% elongation of the normal Si-O long bond length (1.614 $\overset{\circ}{A}$) and is

47

fairly close to some observed Al-O bond lengths (1.78 Å).[17] In fact, this separation is exactly what Nuttall and Weil derived from the near intersection of the Al and Si hyperfine principal directions.

The total unpaired spin density in 3p-type orbitals on the aluminum ion is 0.037, assuming a value of 59 MHz for the interaction of a full 3p orbital with the aluminum nucleus.[18] This spin-density value should only be considered as a relative number since, as stated earlier, dipole-dipole interactions with unpaired spin at the other oxygen ligands would have the same principal directions and hence would reduce this number. Also, the calculated hyperfine of the full 3p orbital depends on the charge assumed for the aluminum ion, i.e., the amount of covalency involved in the complex. (The value of 59 MHz is for a 3p orbital on a neutral aluminum.) It can be seen, however, that only a small amount of unpaired spin in Al 3p orbitals is needed to explain the small anisotropic hyperfine splitting observed for the $[AlO_4]^o$.

The isotropic hyperfine of 16.14 MHz has been explained previously by Barker in terms of core polarization and some unpaired spin in an aluminum 3s orbital due to sp hybridization, and our results here do not affect his explanation.

References

1. N. Koumvakalis, J. Appl. Phys. <u>51</u>, 5528 (1980).

2. J. C. King and H. H. Sander, Radiat. Eff. <u>26</u>, 203 (1975).

3. J. H. E. Griffiths, J. Owen, and I. M. Ward, <u>Report of the Bristol Conference-Defects in Crystalline Solids</u> (The Physical Society, London, 1955), p. 81.

4. M. C. M. O'Brien, Proc. Roy. Soc. (London) <u>A231</u>, 404 (1955).

5. J. H. Mackey, Jr., J. Chem Phys. <u>39</u>, 74 (1963).

6. J. H. Mackey, J. W. Boss, and D. E. Wood, J. Magn. Res. <u>3</u>, 44 (1970).

7. R. Schnadt and J. Schneider, Phys. Kondens. Mater. <u>11</u>, 19 (1970).

8. J. A. Weil, Radiat. Eff. <u>26</u>, 261 (1975).

9. P. R. Barker, J. Phys. C <u>8</u>, L142 (1975).

10. L. E. Halliburton, N. Koumvakalis, M. E. Markes, and J. J. Martin, J. Appl. Phys. <u>52</u>, 3565 (1981).

11. R. H, D. Nuttall and J. A. Weil, Can. J. Phys. <u>59</u>, 1696 (1981).

12. R. H. D. Nuttall and J. A. Weil, Can. J. Phys. <u>59</u>, 1709 (1981).

13. R. H. D. Nuttall and J. A. Weil, Can. J. Phys. <u>59</u>, 1886 (1981).

14. J. D. H. Donnay and Y. Le Page, Acta Crystallogr. Sect. A <u>34</u>, 584 (1978).

15. M. G. Jani, R. B. Bossoli, and L. E. Halliburton, Phys. Rev. B <u>27</u>, 2285 (1983).

16. O. F. Schirmer, Solid State Commun. <u>18</u>, 1349 (1976).

17. J. V. Smith, Acta Crystallogr. <u>7</u>, 479 (1954).

18. J. E. Wertz and J. R. Bolton, <u>Electron Paramagnetic Resonance</u> (McGraw-Hill, New York, 1972), Table C.

TABLE I. Spin-Hamiltonian parameters for the $[AlO_4]^0$ center in α-quartz. The principal values are given in units of MHz.

| | | Principal directions[a] | |
	Principal values	θ	ϕ
A_{AL}/h (present work)	−17.049	90.71°	296.35°
	−17.263	135.54°	205.62°
	−14.062	134.45°	27.05°
Q_{AL}/h (present work)	− 0.6255	120.00°	268.92°
	−0.4325	119.54°	159.83°
	1.0580	135.40°	34.75°
A_{AL}/h (Reference 11)	−17.171	88.03°	298.88°
	−17.339	135.23°	210.87°
	−14.117	134.70°	26.92°
Q_{AL}/h (Reference 11)	−0.623	119.89°	269.32°
	−0.4298	119.74°	160.05°
	1.0527	135.32°	34.75°
A_{AL}/h (Reference 9)	−17.34	–	–
	−17.34	–	–
	−14.08	135.11°	29.78°
Q_{AL}/h (Reference 9)	−0.527	–	–
	−0.527	–	–
	1.054	–	–
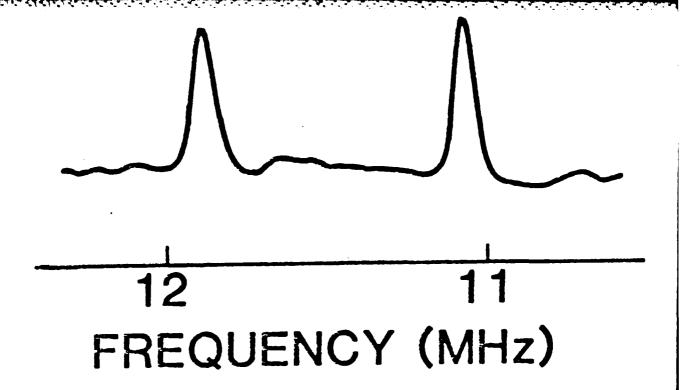
[a]Defined in Reference 15.
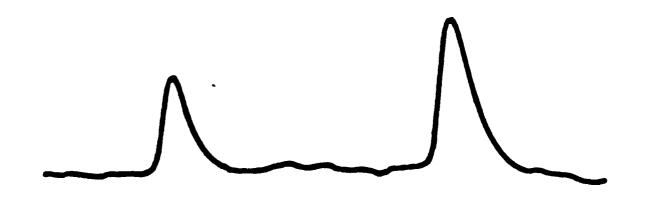
TABLE II. Results obtained from ^{27}Al hyperfine analysis.

Isotropic hyperfine splitting	=	-16.14 MHz
Primary dipole-dipole interaction with hole located on O(3)	=	1.70 MHz

	0.012	(directed toward O(1))
Aluminum 3p-type unpaired spin density	0.014	(directed toward O(2))
	0.011	(directed toward O(4))
TOTAL	0.037	

Figure Captions

1. ENDOR spectrum from the $[AlO_4]^0$ center in alpha-quartz. These data were taken on the fourth line measured relative to the high-field end of the Z-axis ESR spectrum. The magnetic field was 3225.62 G and the microwave frequency was 9.09520 GHz.

2. Projection of the alpha-quartz lattice on the plane perpendicular to the X axis of the crystal.

3. Angular variation of the ^{27}Al hyperfine splitting for rotation in the X plane. The solid curves are calculated from the experimental hyperfine matrix A and the filled circles are our "theory" values.
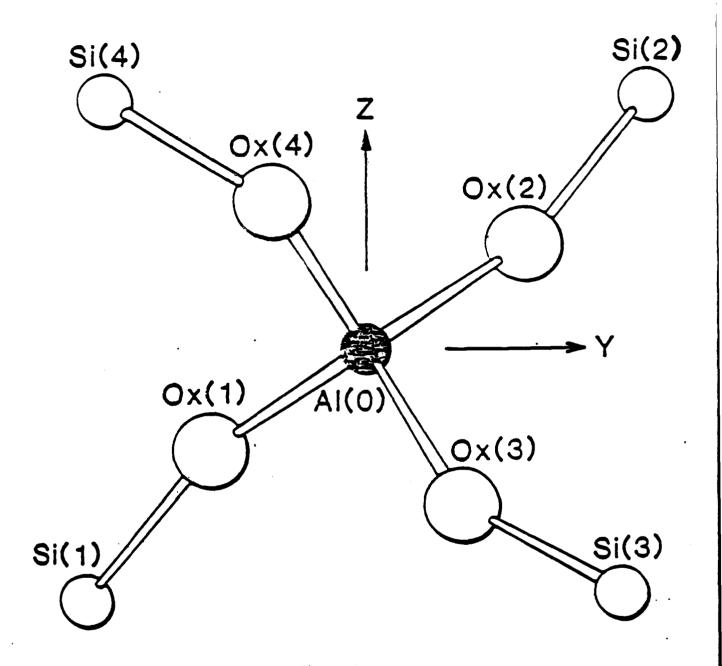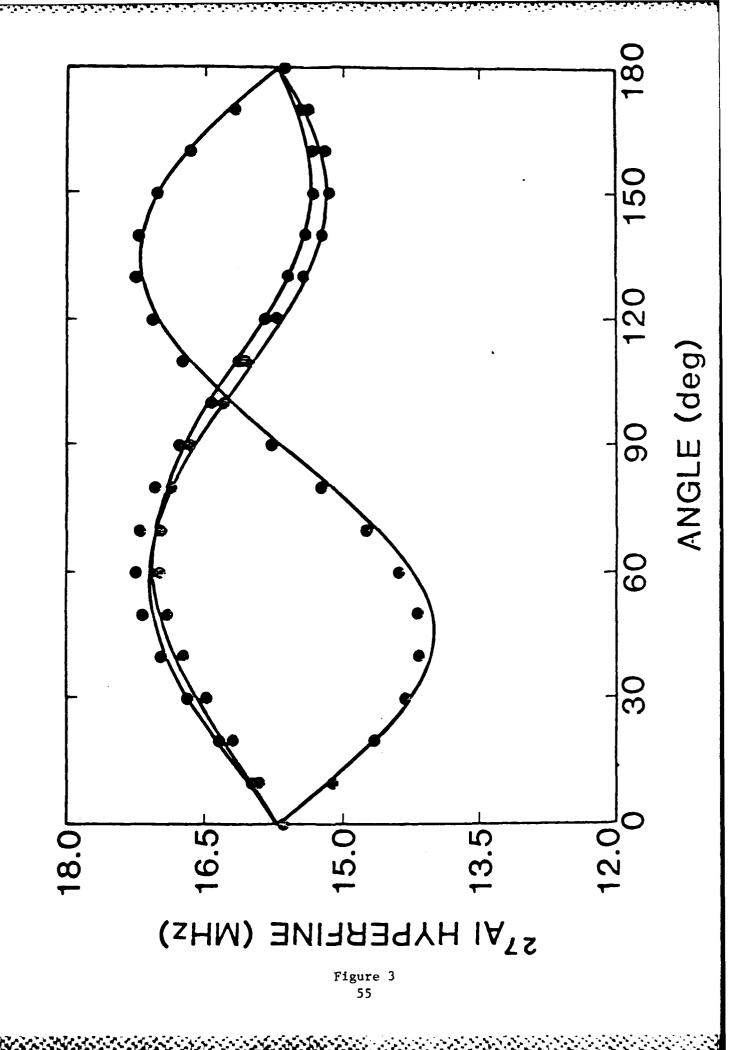
FREQUENCY (MHz)

FREQUENCY (MHz)

Figure 1
53

Figure 2

54

Figure 3

55

V. ELECTRON SPIN RESONANCE AND OPTICAL STUDIES
OF OXYGEN VACANCY CENTERS IN QUARTZ

Introduction

Oxygen-vacancy-associated centers form an important class of defects in alpha-quartz. They are usually referred to as E centers, with E_1', E_2', E_4', E_1'', E_2'', and E_3'' centers being included in this family of defects. The single or double prime as a superscript denotes whether there is one or two unpaired electrons (i.e., S = 1/2 or S = 1) associated with the specific center and the subscripts distinguish between various centers having each spin. In addition to quartz, E centers have been found in silica[1] and the SiO_2 interface region of MOS devices[2] and, in both cases, are believed to be a major feature of the defect structure of the material.

Much of our present understanding of this group of defects has resulted from electron-spin-resonance (ESR) investigations. Among the characteristic features of E-center ESR spectra are very narrow linewidths (less than 0.1 gauss), g values slightly less than 2.0023, and long spin-lattice-relaxation times (which cause severe microwave power saturation effects even at room temperature). In the present paper, we survey the current status of defect models for oxygen-vacancy centers in alpha-quartz. Specific attention is given to the E_1', the E_4', and the three E'' centers. Also, brief consideration is given to the origins of ultraviolet (i.e., the 190 to 300 nm range) absorption bands in quartz. Our discussion is limited to bulk crystalline effects.

Fig. 1 is a projection of the alpha-quartz lattice on the plane perpendicular to the X axis of the crystal. We shall use this figure and its labeling of ions to discuss the various models for E-type centers. As illustrated, each silicon ion has four oxygen neighbors making a slightly distorted tetrahedron and each oxygen ion is bonded to two silicon ions. The four silicon-oxygen bonds can be divided into two types; Si(0) to O(1) and Si(0) to O(2) are short bonds (1.6071 Å) while Si(0) to O(3) and Si(0) to O(4) are long bonds (1.6122 Å). Additional information on the position coordinates of the ions in Fig. 1 are given by Jani et al.[3]

E_1' Centers

The E_1' center was the first of the E-type defects to be systematically investigated in alpha-quartz. Weeks[4] initially observed the ESR spectrum of this center and Silsbee[5] later completed a study of its angular dependence. Spin-Hamiltonian parameters for the g matrix, a strong hyperfine matrix, and two weak hyperfine matrices were reported by Silsbee. In both of these early investigations, fast-neutron irradiation was used to produce the E_1' centers.

The c-axis ESR spectrum of the E_1' center is shown in Fig. 2. A large central line represents those E_1' centers having no resolved hyperfine while the three less intense pairs of lines centered on the main line represent hyperfine interactions of the E_1' centers with three distinct ^{29}Si neighboring nuclei. One of

the hyperfine pairs has a splitting of approximately 403.6 gauss
while the other two pairs have much smaller splittings of 8.02
and 9.12 gauss. Recent ENDOR results by Jani et al.[3] have
verified that these two weak hyperfine splittings are due to ^{29}Si
nuclei. The relative intensities of the primary line and the
hyperfine lines are determined by the 4.7% natural abundance of
the ^{29}Si nucleus, but the rate at which the hyperfine lines shift
with angle (i.e., their sensitivity to magnetic field alignment)
and variations in linewidth may affect the actual intensity
ratios.

The four spin-Hamiltonian matrices determined from the
angular dependence of the E_1' center greatly help in the
developing of a correct model for the defect.[3,5] Each of the
four matrices (the g and three hyperfine) is nearly axial. The
unique axes of the g matrix and strong (i.e., 400-gauss
magnitude) hyperfine matrix coincide with each other and are
parallel to a short-bond silicon-oxygen direction in the perfect
quartz lattice. The unique axes of the two weak hyperfine
interactions also can be associated with specific bond directions
in the lattice, although the agreement is not as striking as in
the case of the previous two matrices.[3] More will be said later
in this section about the impact on the E_1' center model of the
assignment of specific silicon sites to these two weak hyperfine
interactions.

The presently accepted model of the E_1' center has resulted
from the theoretical work of Feigl et al.[6] and Yip and Fowler.[7]
Their calculations support a model consisting of an oxygen
vacancy with an unpaired electron localized in the sp^3 hybrid

orbital extending into the vacancy from an adjacent silicon ion. An important feature of their model is an asymmetrical relaxation of the two silicon ions nearest the vacancy, the silicon with the unpaired electron moves toward the vacancy and the opposite silicon moves away from the vacancy. In terms of the labeling used in Fig. 1, if oxygen O(1) were missing the unpaired electron would extend into the vacancy from Si(0), with Si(0) relaxing toward the vacancy and Si(1) moving away from the vacancy. Initial calculations[7] indicated the unpaired electron should be associated with the silicon ion having the long bond to the missing oxygen ion. However, later calculations by Edwards[8] have shown that the minimum energy configuration corresponds to having the unpaired electron on the short-bond side of the vacancy, a result which is in agreement with experiment.

In the single-vacancy model of Feigl, Fowler, and Yip, it is difficult to identify the two silicon sites responsible for the 8 and 9 gauss hyperfine splittings observed in the E_1' center ESR spectrum. Referring to Fig. 1 again, there is Si(1) located on the opposite side of the vacancy from the unpaired electron or there are the three silicons bonded to Si(0) through the oxygen ions O(2), O(3), and O(4). Neither case gives two, and only two, nearly equivalent weakly interacting silicon nuclei. Jani et al.[3] have determined that the unique axis directions of the two weak hyperfine matrices show reasonable agreement with the Si(2) to O(2) and the Si(3) to O(3) bond directions in the perfect lattice. Based on this evidence, Jani et al.[3] have proposed a modification of the Feigl, Fowler, and Yip model of the E_1' center

that incorporates a second oxygen vacancy. A divacancy model of
the E_1' center had earlier been suggested by Weeks.[9] In terms of
Fig. 1, the specific model proposed by Jani et al. would have
oxygen vacancies at O(1) and O(4), an unpaired electron localized
on Si(0) and extending toward vacancy O(1) in an sp^3 orbital, and
weak hyperfine interactions with Si(2) and Si(3) via super-
exchange through the intervening oxygens. As an alternative to
the second oxygen vacancy proposal, Griscom and Friebele[10] have
suggested that a peroxy-type molecular ion (e.g., O_2^{2-}) might
occupy the O(4) site and significantly decrease the hyperfine
interaction with Si(4).

Production characteristics also indicate that the E_1' center
in quartz may be complex. Electron irradiation (1.7 MeV) at room
temperature does not directly produce significant numbers of E_1'
centers in high-quality synthetic quartz. However, *if the*
crystal is heated to approximately 300°C after the room-
temperature irradiation, more than an order of magnitude
enhancement in the concentration of E_1' centers is observed.[11-13]
The results shown in Fig. 3 are from the thermal anneal of a
quartz crystal irradiated at room temperature and then further
irradiated at 77 K. Growth of the E_1' centers in the 200-300°C
range coincides with the decay of aluminum-hole centers, also
known as $[AlO_4]^0$ centers. After being formed in the previously
irradiated crystal by annealing to 300°C, the E_1' centers then
thermally decay in the 300-350°C region. Additional
investigation has revealed a dependence on irradiation
temperature for the formation of E_1' centers.[3] Considerably fewer
E_1' centers are created by the thermal anneal to 300°C after only

an initial irradiation at 77 K than if the crystal had been irradiated initially at room temperature. In general, it has been found that a maximum concentration of E_1' centers is created by a 300°C anneal only if the crystal has been previously irradiated at a temperature above 200 K. It is of interest that interstitial alkali ions become mobile under irradiation at this same temperature of 200 K.[14]

The nature of possible precursor states to the E_1' center, the possible role of aluminum-hole centers and alkali mobility, and other details of the formation mechanisms for E_1' centers are not well understood at the present time. Also, the model of the E_1' center must receive more attention, both theoretically and experimentally. Future investigations must address these and other questions about this important defect.

E_4' Centers

The E_4' center is an oxygen-vacancy-associated defect which is similar to the E_1' center except that it shows a well resolved hyperfine pattern from a 100% abundant nucleus. Weeks and Nelson were the first to report this defect.[11] Fig. 4a is the c-axis ESR spectrum of the E_4' center taken at 9.1 GHz. The spectrum at this microwave frequency consists of four primary lines nearly equally split and equally intense. This appearance of the ESR spectrum prompted the early investigators to suggest a 100% abundant $I = 3/2$ nucleus as the origin of the observed splittings. Usually, there are $(2I+1)$ lines in a hyperfine

61

pattern and this is the basis of the I = 3/2 assignment.

However, more recent work has shown that the nucleus responsible for the primary hyperfine splitting of the E_4' center is hydrogen, i.e., an I = 1/2 spin.[15] This is verified by the c-axis ESR spectrum taken at 20.4 GHz and shown in Fig. 4b. The splitting for the outer pair of lines increases significantly with microwave frequency and their intensity decreases. The spectra in Fig. 4 are explained by assuming an S = 1/2, I = 1/2 spin system and a spin-Hamiltonian containing three terms, electron Zeeman, hyperfine, and nuclear Zeeman. Near 9 GHz, the hyperfine and nuclear Zeeman terms are comparable in magnitude and there is a major amount of mixing between the $|M_S,m_I\rangle$ states of the system. This introduces observable "forbidden" transitions and gives rise to the four lines found in Fig. 4a. At 20 GHz, the magnitude of the nuclear Zeeman term has increased and it is no longer comparable to the hyperfine term.

A detailed angular-dependence study of the E_4' center has been reported by Isoya et al.[16] In addition to the weak hydrogen hyperfine, they found large hyperfine interactions with two ^{29}Si nuclei. This is in contrast to the E_1' center which had a large hyperfine interaction with only one ^{29}Si nucleus. The g matrix, proton hyperfine matrix, and two strong silicon hyperfine matrices for the E_4' center are very nearly axial. Knowing the direction of the unique principal axis for each of these matrices, Isoya et al.[16] constructed a model for the defect. Specifically, they suggested that a hydride ion (H$^-$) is trapped in an oxygen vacancy with an additional unpaired electron being shared unequally by the two silicon ions neighboring the vacancy.

In terms of Fig. 1, if O(1) were missing then the hydride ion would be in the vacancy and preferentially bonded to Si(0). The strong hyperfine interactions would be with Si(1) and Si(0), the larger being with Si(1). Variations with temperature of the E_4' center spin-Hamiltonian parameters were observed which suggest significant temperature-dependent ionic distortions of the center and related electronic structure changes.

Isoya et al.[16] provided additional support for their proposed E_4' center model by calculating the equilibrium ionic and electronic structure for such a model using the ab initio SCF-MO computer program known as Gaussian 70.[17] The 15-atom cluster $Si_2O_6H_7$, with the oxygen vacancy at the center and including six terminating hydrogens on the outer six oxygens, was investigated. The central hydrogen and two silicons were allowed to move while the program searched for a minimum energy configuration. Given the limitations of the theory model, surprisingly good agreement was obtained between the calculations and experiment.

E″ Centers

The defects, which are now labeled E″ centers, were first reported by Weeks and Abraham[18,19] and later were briefly described by Solntsev et al.[13] More recently, Bossoli et al.[20] have provided a detailed description of the production and thermal decay properties of these E″ centers and Jani[21] has investigated the angular dependence of their ESR spectra. These defects are S = 1 centers but otherwise have all of the

characteristics previously associated with the $S = 1/2$ E_1' centers. That is to say, the E'' centers have g values slightly less than 2.0023, narrow linewidths, equivalent 400-gauss magnitude hyperfine interactions with silicon nuclei, and long spin-lattice relaxation times. Thus, by analogy, the E'' centers are thought to be associated with oxygen vacancies.

The relatively complex set of production criteria described by Bossoli et al.[20] for the E'' centers is very similar to that found by Jani et al.[3] for the E_1' centers. The E'' centers are easily produced in synthetic and natural quartz by ionizing radiation provided certain conditions are met. A 77-K irradiation of a previously unirradiated unswept sample does not produce an appreciable number of E'' centers. However, the E'' centers are easily produced by a 77-K irradiation of an unswept sample, if the sample has been previously irradiated at room temperature. Bossoli et al. also report that the E'' centers are difficult to produce in hydrogen-swept samples, independent of whether the sample had been pre-irradiated at room temperature.

Fig. 5 shows the ESR spectra of the E'' centers. The magnetic field is parallel to the c axis and each of the three E'' centers appears as a doublet. Magnetic field splittings are 5.01, 11.02, and 17.88 gauss for the E_1'', E_2'', and E_3'' doublets, respectively, and their g_c values are all near 2.0010. Approximately centered on each of these primary doublets are eight less intense hyperfine lines, four at higher field and four at lower field.[20] The four hyperfine pairs for each of the E'' centers are split by roughly 200 gauss and are due to strong hyperfine interactions with two slightly inequivalent ^{29}Si

nuclei.[21] These latter hyperfine splittings are about one-half of the equivalent strong ^{29}Si hyperfine splitting for the E_1' center and this indicates, after accounting for the factor-of-two reduction introduced by the S = 1 spin system, that the strong interactions with silicon nuclei are comparable for the E'' and E' centers. Thus, there must be similarities in the electronic structure of the two types of centers.

Fig. 6 illustrates the thermal stability of the E'' centers. The crystal was electron irradiated at room temperature and then at 77 K to produce the E'' centers. Then an isochronal pulse-anneal was performed from 8 to 100°C with the ESR spectra being recorded at 8°C after a 5-minute anneal at each elevated temperature. The E_2'' centers were found to anneal near 50°C while the E_1'' and E_3'' centers annealed near 85°C and 95°C, respectively. Further production studies by Bossoli et al.[20] revealed that E'' centers were not created in significant concentrations whenever interstitial alkali ions were located adjacent to the substitutional aluminum ions. Most likely, this means that the formation of $[AlO_4]^{\circ}$ centers plays a precursor role in the formation mechanisms for E'' centers.

To a first approximation, the E'' centers can be viewed as two neighboring E_1' centers. The three slightly different E'' centers would then result from the various geometries possible for neighboring oxygen vacancies in the complex quartz lattice. This general model for these centers is supported by the values of electron separation obtained from the dipole-dipole interactions (i.e., maximum fine-structure splitting in the

65

angular dependence).[21]

UV Optical Absorption

Considerable experimental work was done during the 1950s and 60s on ultraviolet absorption bands in quartz. Except for the theoretical studies of Griscom and Fowler[22] and Schirmer,[23] very little attention has been given to this area recently. In the initial investigations, Mitchell and Paige[24,25] measured the optical absorption of neutron and x-ray irradiated quartz in the wavelength range 145 to 1000 nm. They observed two major bands in the UV region, at 217.5 and 163.1 nm, and labeled them the C and E bands, respectively. Their evidence suggested that the C band might be due to an electron trapped in an oxygen vacancy and that the E band might be due to the related interstitial oxygen ion.

Nelson and Crawford[26] examined the optical absorption of neutron-irradiated quartz over the range 185 to 2600 nm and found a band near 215 nm which appeared to be the same as the C band of Mitchell and Paige. The complex character of this 215 nm band was noted by Nelson and Crawford; their data supports the view of Levy[27] that the C-band is a composite of several independent bands. Nelson and Crawford suggested that this absorption was associated with vitreous regions of the crystal produced by the neutron bombardment. Nelson and Weeks[28] studied ^{60}Co gamma-irradiated quartz and found a correlation between an optical band at 230 nm and the E_2' center.[9,11]

Arnold[29] irradiated quartz with 2-MeV electrons at

temperatures near 77 K and produced an optical absorption band at 220 nm (i.e., the C band). He concluded that the defect giving rise to the C band is a result of a displacement process, but that the production rate of the defect increases with faster crystal growth rates. In a second paper, Arnold[30] attributed the C band to displacement of oxygen ions and determined that the threshold energy for this displacement varied from 15 eV for fast-grown quartz to 50 eV for slow-grown material.

There is a significant need for additional experimental studies of ultraviolet optical absorption bands in quartz. An important feature of this future work must be an emphasis on correlating optical and ESR data, especially now that a better understanding of the E-type ESR spectra is available. In initial efforts at Oklahoma State University, we have failed to find correlations between absorption bands in the 190 to 300 nm region and the various paramagnetic E centers.

References

1. E. J. Friebele and D. L. Griscom, in: Treatise on materials science and technology, Vol. 17, ed. M. Tomozawa and R. Doremus, (Academic Press, New York, 1979) pp. 257-351.

2. D. L. Griscom, in: The physics of SiO_2 and its interfaces, ed. S. T. Pantelides, (Pergamon Press, Elmsford, NJ, 1978) pp. 232-252.

3. M. G. Jani, R. B. Bossoli and L. E. Halliburton, Phys. Rev. B 27 (1983) 2285.

4. R. A. Weeks, J. Appl. Phys. 27 (1956) 1376.

5. R. H. Silsbee, J. Appl. Phys. 32 (1961) 1459.

6. F. J. Feigl, W. B. Fowler and K. L. Yip, Solid State Commun. 14 (1974) 225.

7. K. L. Yip and W. B. Fowler, Phys. Rev. B 11 (1975) 2327.

8. A. H. Edwards, Ph.D. Dissertation, Lehigh University (1981).

9. R. A. Weeks, Phys. Rev. 130 (1963) 570.

10. D. L. Griscom and E. J. Friebele, private communication.

11. R. A. Weeks and C. M. Nelson, J. Am. Ceram. Soc. 43 (1960) 399.

12. F. J. Feigl and J. H. Anderson, J. Phys. Chem. Solids 31 (1970) 575.

13. V. P. Solntsev, R. I. Mashkovtsev and M. Ya. Schlerbakova, Zh. Strukt. Khim. 18 (1977) 729 [J. Struct. Chem. (USSR) 18 (1977) 578].

14. M. E. Markes and L. E. Halliburton, J. Appl. Phys. 50 (1979) 8172.

15. L. E. Halliburton, B. D. Perlson, R. A. Weeks, J. A. Weil and M. C. Wintersgill, Solid State Commun. 30 (1979) 575.

16. J. Isoya, J. A. Weil and L. E. Halliburton, J. Chem. Phys. 74 (1981) 5436.

17. W. J. Hehre, R. F. Stewart and J. A. Pople, J. Chem. Phys. 51 (1969) 2657;

    W. J. Hehre, R. Ditchfield, R. F. Stewart and J. A. Pople, J. Chem. Phys. 52 (1970) 2769.

18. R. A. Weeks and M. M. Abraham, Oak Ridge National Laboratory report Solid State Division Annual Proress Report (1964) 36.

19. R. A. Weeks and M. M. Abraham, Bull. Am. Phys. Soc. 10 (1965) 374.

20. R. B. Bossoli, M. G. Jani and L. E. Halliburton, Solid State Commun. 44 (1982) 213.

21. M. G. Jani, Ph.D. Dissertation, Oklahoma State University (1982).

22. D. L. Griscom and W. B. Fowler, in: The physics of MOS insulators, ed. G. Lucovsky, S. T. Pantelides, and F. L. Galeener, (Pergamon Press, New York, 1980) pp. 97-101.

23. O. F. Schirmer, in: The physics of MOS insulators, ed. G. Lucovsky, S. T. Pantelides, and F. L. Galeener, (Pergamon Press, New York, 1980) pp. 102-106.

24. E. W. J. Mitchell and E. G. S. Paige, Proc. Phys. Soc. (London) B67 (1954) 262.

25. E. W. J. Mitchell and E. G. S. Paige, Phil. Mag. 1 (1956) 1085.

26. C. M. Nelson and J. H. Crawford, J. Phys. Chem. Solids 13 (1960) 296.

27. P. W. Levy, Bull. Am. Phys. Soc. 1 (1956) 136.

28. C. M. Nelson and R. A. Weeks, J. Am. Ceram. Soc. 43 (1960) 396.

29. G. W. Arnold, Phys. Rev. 139A (1965) 1234.

30. G. W. Arnold, Phys. Rev. 140A (1965) 176.

Figure Captions

1. Projection of the alpha-quartz lattice on the plane perpendicular to the X axis of the crystal.

2. ESR spectrum of the E_1' center in quartz. The data were taken at room temperature with the magnetic field parallel to the c axis and a microwave frequency of 9.3358 GHz. Amplification of the center line was a factor of 10 less than for the hyperfine lines.

3. Thermal anneal behavior of a sample initially irradiated at room temperature and then at 77 K. Following each 15-minute anneal step, the E_1' centers and $[AlO_4]^0$ centers were monitored at room temperature and 77 K, respectively.

4. Room-temperature ESR spectra of the E_4' center in quartz taken at 9.1 GHz (trace a) and 20.4 GHz (trace b). The magnetic field is parallel to the c axis in both cases.

5. Room-temperature ESR spectra from the E_1'', E_2'', and E_3'' centers in quartz taken at 9.3092 GHz with the magnetic field parallel to the c axis.

6. Thermal stability of the E'' centers in a 77-K irradiated sample. The intensity of each defect was monitored at 8^oC after each 5-minute anneal step.
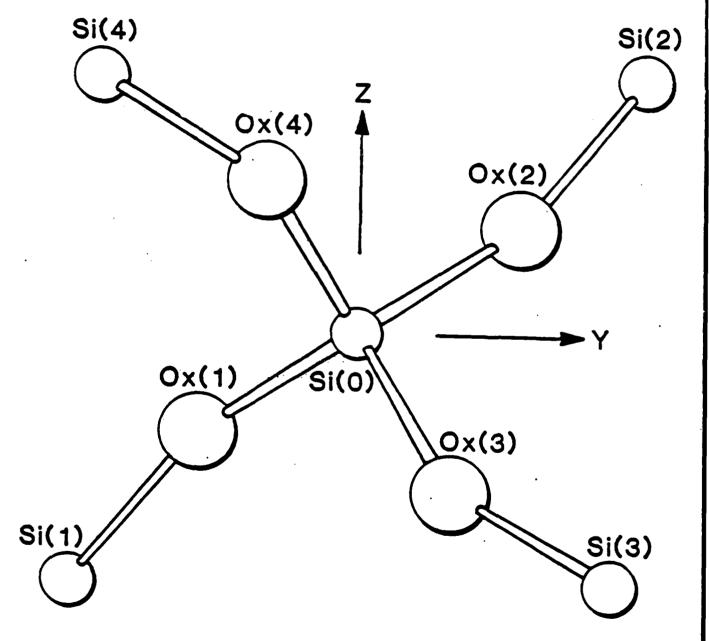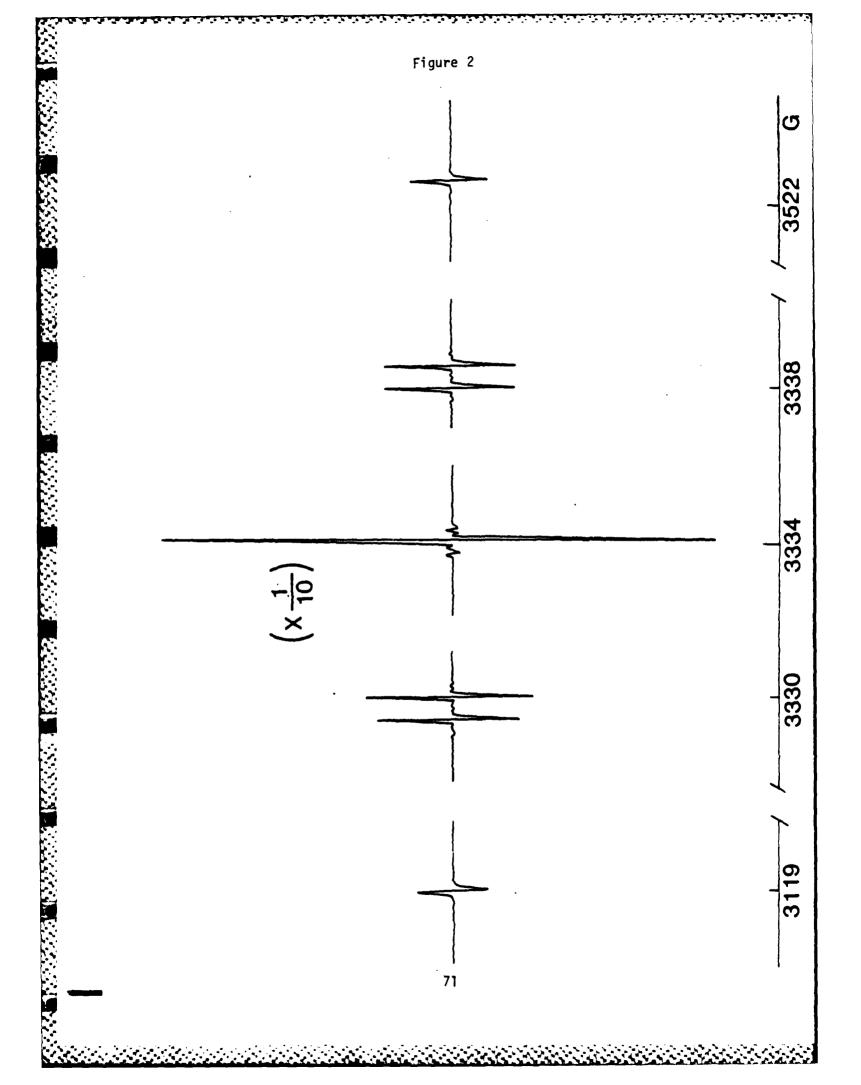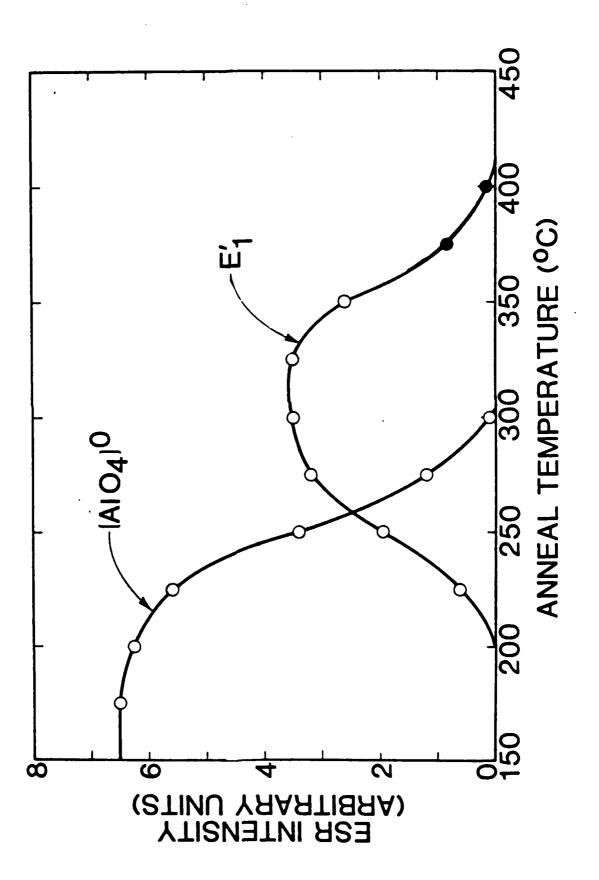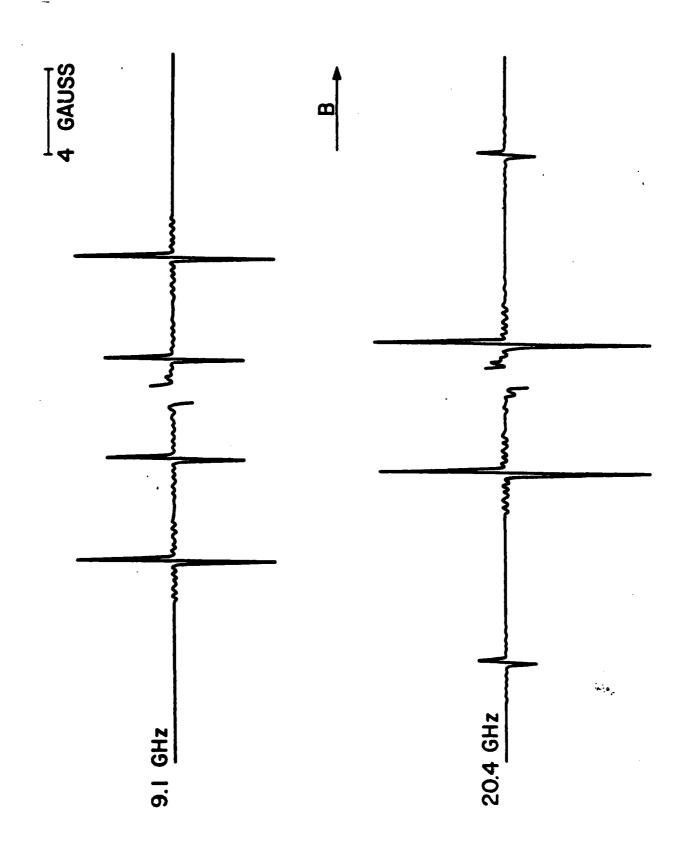
Figure 1

70

Figure 2

$\left(x\frac{1}{10}\right)$

3119   3330   3334   3338   3522   G

71

Figure 3

Figure 4

4 GAUSS

B

9.1 GHz

20.4 GHz

73

Figure 5

74
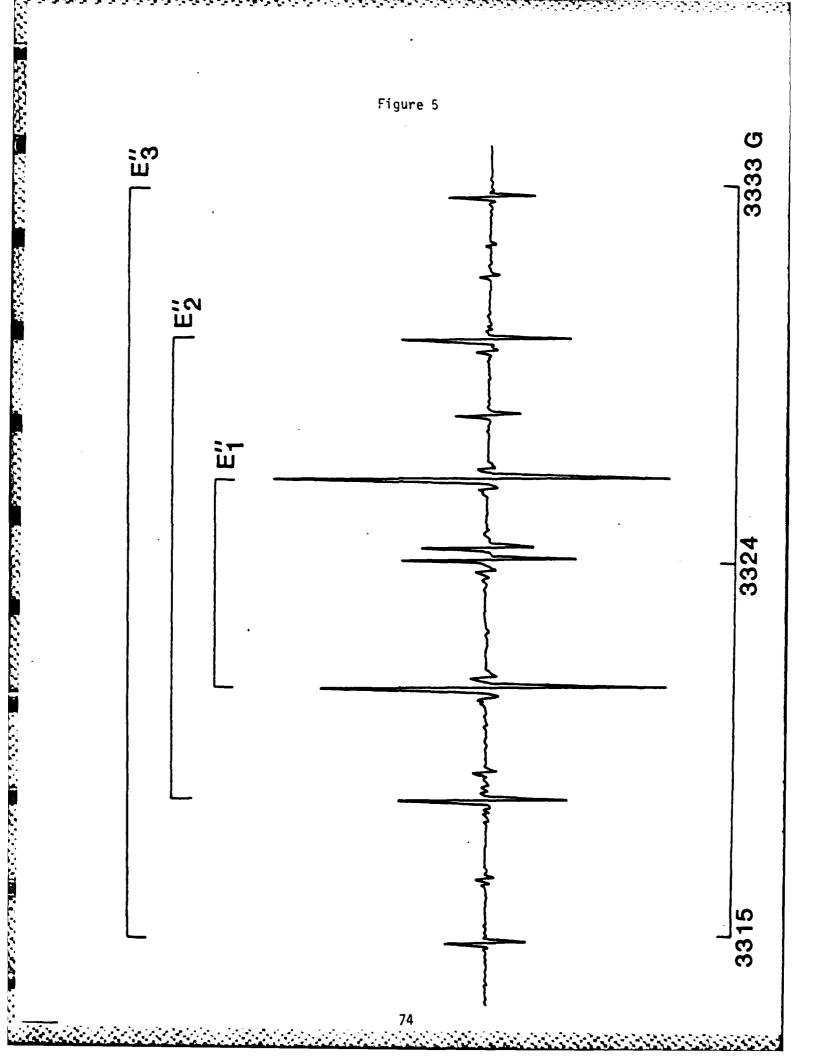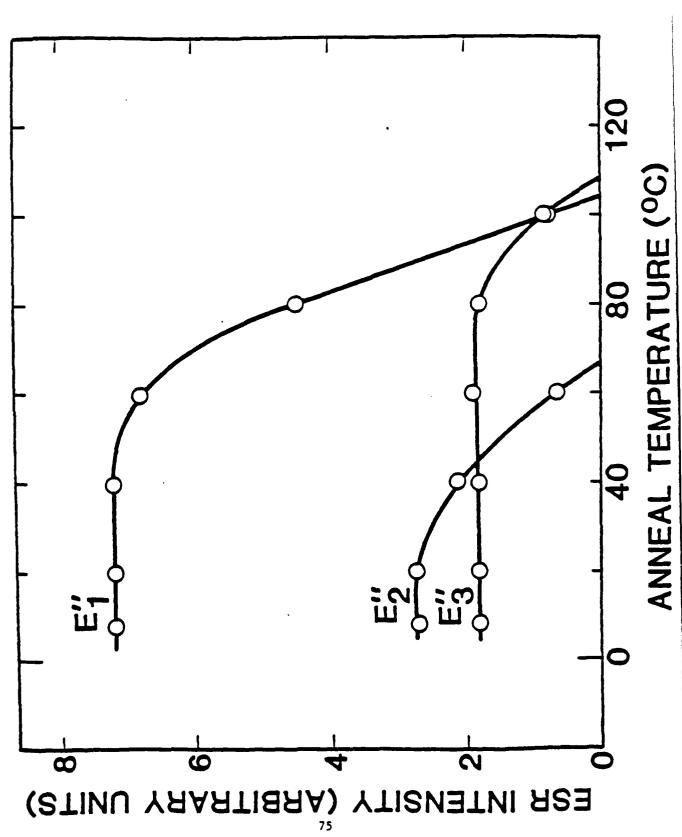
Figure 6

Figure 6

VI. RADIATION-INDUCED MOBILITY OF LITHIUM
AND SODIUM IN ALPHA-QUARTZ

Introduction

Alpha-quartz usually contains aluminum as a substitutional impurity. In as-grown material, the substitutional Al^{3+} is charge compensated by an adjacent interstitial alkali ion. The resulting $Al-M^+$ center, where M^+ represents Li^+ or Na^+, plays a vital role in the radiation response of quartz.[1] A recent series of papers has established that the alkali ion only becomes mobile (i.e., is dissociated from the aluminum) under ionizing radiation if the sample is at a temperature above approximately 200 K.[2,3,4] As the alkali ion leaves the aluminum site, it is replaced by either a hole or a proton on an adjacent non-bonding oxygen orbital. The alkali drifts along the Z-axis channel and is subsequently trapped at an as-yet unidentified site. The protons, which replace many of the alkalis, come from the OH^--related defects that are responsible for the infrared absorption bands at 3585, 3437, and 3400 cm^{-1}. The resulting $Al-OH^-$ centers give rise to the 3367 and 3306 cm^{-1} absorption bands [5,6,7] and can be used to monitor this radiation-induced mobility of the alkali ions.[2]

In as-grown synthetic quartz the alkali ions are thought to be a mixture of sodium and lithium. However, Martin et al.[8] have recently found Li^+ is the majority charge-compensating alkali ion in high quality material grown with the addition of a small amount of Li_2CO_3 to the Na_2CO_3 mineralizer. Electrodiffusion

(sweeping), introduced by King,[9] can be used to change the concentration of specific charge-compensating ions. Kats[5] used the technique to "sweep" hydrogen and alkalis into and out of quartz. Fraser[10] has described the basic technology for sweeping alkalis. We report here an infrared investigation of the radiation-induced mobility of Li^+ and Na^+ ions using electro-diffused samples of synthetic quartz.

Experimental Procedure

Z-plate optical samples, 15 mm square by 3 mm thick, were cut from unswept pure z-growth synthetic quartz. Sample SQ-B4 was from a Toyo Supreme Q bar while samples PQ-E21 and EG-E50 were from Sawyer Premium Q and Electronic Grade bars, respectively. All infrared scans were made with a Beckman 4240 infrared spectrophotometer. A Dewar containing liquid nitrogen held the sample at 80 K during the IR measurements. All irradiations were carried out with 1.7-MeV electrons from a Van de Graaff accelerator. The current density on the samples was approximately 1.7 $\mu A/cm^2$. The sample was maintained at the desired temperature, between 80 K and RT, in the optical Dewar and irradiated for 2 minutes on each side through the Dewar's aluminum foil radiation port. Past experience has shown that this dose is sufficient to saturate (i.e., reach the maximum concentration) the aluminum-related defects. After each infrared scan, the sample was raised to the desired temperature, then irradiated, and finally cooled back to 80 K for the next infrared

scan. Since the 3367 and 3306 cm^{-1} Al-OH$^-$ bands have nearly the same half-widths,[2] the sum of their absorption coefficients was used to determine the conversion of the Al-M$^+$ centers into the Al-OH$^-$ centers.

The alkali sweeping consisted of vapor-depositing a NaCl or LiCl film on one side of the optical samples, as the source electrode, and subsequently depositing Au electrodes on both sides. The sample was then mounted in a graphite holder, placed in a vacuum furnace, and raised to 480°C. An electric field of 10 to 20 V/cm was applied to sweep the alkali ions from the film into the crystal. The sweep was continued until a sufficient number of ions were transported; this usually took less than two hours. The sample was then cooled back to room temperature with the field on to prevent back diffusion. After the Au electrodes were removed, an infrared scan was made at 80 K to verify that no hydrogen was swept into the sample. Then the variable temperature irradiation sequence was initiated.

Results and Discussion

The squares in Fig. 1 show the growth of the Al-OH$^-$ center as a function of irradiation temperature for unswept sample SQ-B4. After sample SQ-B4 was electrodiffused with sodium, the growth curve (represented by the circles) shifted to higher temperatures as shown in Fig. 1 and the Al-OH$^-$ centers saturated at a lower concentration in the Na-swept condition. Similar curves were observed for sample PQ-E21, but were omitted from Fig. 1 for clarity. Sample PQ-E21 also showed a similar lower

saturation when Na-swept than when it was in the unswept condition. After the Na-swept run, sample SQ-B4 was Li-swept. The results shown in Fig. 1 for sample SQ-B4 in the Li-swept condition, represented by triangles, are the same as the original unswept results.

We see that the sweeping in of Na^+ shifts the curve to slightly higher temperatures and lowers the maximum number of Al-OH^- centers. A subsequent Li^+ sweep returns the sample to its original unswept condition. Acoustic loss measurements[8] on resonator crystals fabricated from Sawyer bar PQ-E show that Li^+ is the dominant charge compensator in this material. The results shown in Fig. 1 for the unswept and Li^+-swept condition suggest that Li^+ is the majority charge compensator in Toyo bar SQ-B. The difference between the maximum number of Al-OH^- centers that we are able to produce by radiation in the Li^+-swept and Na^+-swept states is not understood. If we normalize the Li^+-swept and Na^+-swept curves shown in Fig. 1 to their respective saturation values, the results shown in Fig. 2 are obtained. Figure 2, and similar curves for sample PQ-E21, show that Na^+ is released from the Al site at temperatures 10-15 K higher than the release of Li^+.

Sawyer Electronic Grade quartz contains substantially more OH^--related defects than either Sawyer Premium Q or Toyo Supreme Q material.[1,2] Figure 3 shows the normalized growth of the Al-OH^- center as a function of the irradiation temperature for the Electronic Grade sample EG-E50 after first a Na^+ sweep and then a Li^+ sweep. Again Li^+ becomes mobile approximately 10-15 K before

79

Na^+. However, the unswept curve, which was omitted for clarity, lies between the Li^+-swept and the Na^+-swept results. This suggests that Electronic Grade material contains a significant amount of Na^+ as the charge compensating ion. Doherty et al.[4] observed a fairly large 50-K Na-related acoustic loss peak in Electronic Grade resonators, which they were able to enhance by electrodiffusion of Na^+.
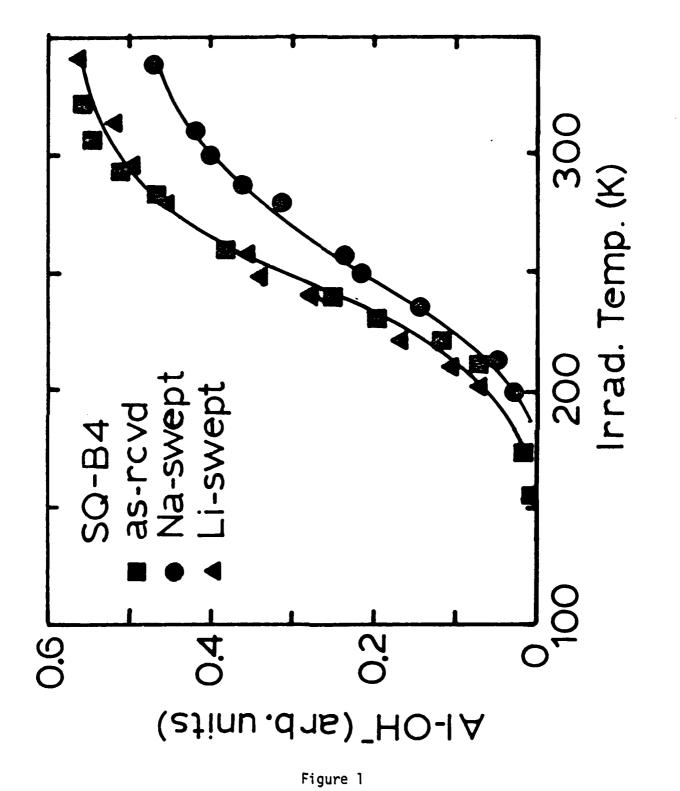
Ionizing radiation creates mobile electrons and holes in the quartz lattice, and the charge compensating alkali is probably thermally released from the aluminum site when a hole interacts with the $Al-M^+$ center. This would suggest that the lighter, smaller Li^+ ion should be released at somewhat lower tempratures than Na^+. The difference in saturation level of the $Al-OH^-$ center in Li^+ and Na^+-swept material is not understood.

References

1. L. E. Halliburton, N. Koumvakalis, M. E. Markes, and J. J. Martin, J. Appl. Phys. $\underline{52}$, 3565 (1981).

2. W. A. Sibley, J. J. Martin, M. C. Wintersgill, and J. D. Brown, J. Appl. Phys. $\underline{50}$, 5449 (1979).

3. M. E. Markes and L. E. Halliburton, J. Appl. Phys., $\underline{50}$, 8172 (1979).

4. S. P. Doherty, J. J. Martin, A. F. Armington, and R. N. Brown, J. Appl. Phys. $\underline{51}$, 4164 (1980).

5. A. Kats, Philips Res. Rpts. $\underline{17}$, 133 (1962).

6. D. M. Dodd and D. B. Fraser, J. Phys. Chem. Solids $\underline{26}$, 673 (1965).

7. H. G. Lipson, A. Kahan, R. N. Brown, and F. K. Euler, Proceedings of the 35th Annual Symposium on Frequency Control (1981), p. 329.

8. J. J. Martin, L. E. Halliburton, R. B. Bossoli, and A. F. Armington, Proceedings of the 36th Annual Symposium on Frequency Control (1982), p. 77.

9. J. C. King, Bell System Tech. J. $\underline{38}$, 573 (1959).

10. D. B. Fraser, J. Appl. Phys. $\underline{35}$, 2913 (1964.)

Figure Captions

1. The growth of the Al-OH$^-$ band as a function of sample temperature during irradiation for Toyo Supreme Q sample SQ-B4 is shown. Sweeping Na$^+$ shifts the curve to higher temperatures and lowers the maximum Al-OH$^-$ concentration. A subsequent Li$^+$ sweep restores the sample to the "unswept" condition.

2. The normalized growth curves for sample SQ-B4 after Na$^+$ sweeping and a subsequent Li$^+$ sweep are shown. Li$^+$ is released from the aluminum site 10-15 K below the release of Na$^+$.

3. Normalized growth curves for the Al-OH$^-$ center as a function of irradiation temperature in Sawyer Electronic Grade sample EG-E50 are shown. Again the Li$^+$-swept curve is at lower temperature. The initial unswept results which were omitted for clarity were between the Li$^+$ and Na$^+$-swept curves.
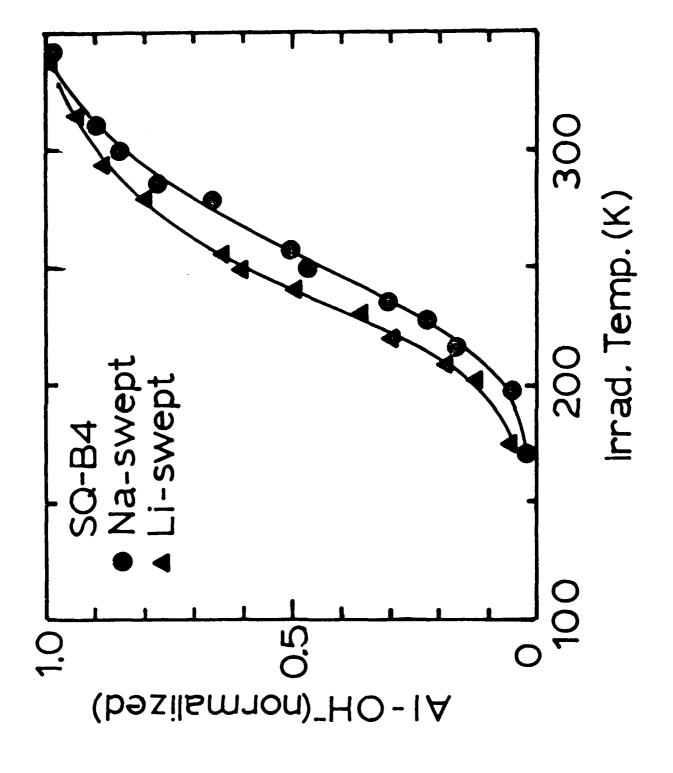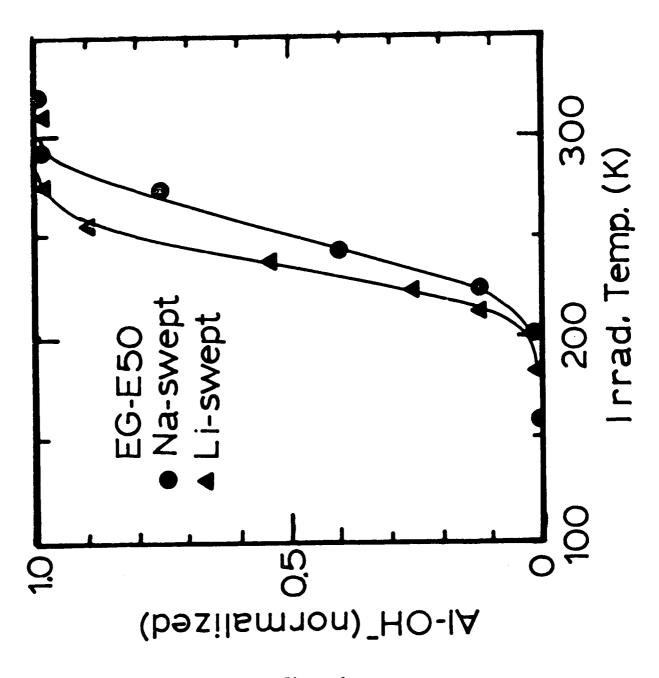
Figure 1

83

Figure 2

Figure 3

85

VII. THERMALLY STIMULATED LUMINESCENCE ABOVE
ROOM TEMPERATURE IN QUARTZ

Introduction

Thermally stimulated luminescence (TSL) is a sensitive
technique used to characterize point defects in wide-bandgap
materials.[1,2] The experiment consists of irradiating a sample to
produce various defects and then heating at a constant rate while
monitoring any emitted light due to charge recombination. As
characteristic temperatures are reached, specific defects will
become unstable and release charge which then recombines with
opposite charge at other defect sites. The temperatures of these
"glow peaks", their associated activation energies, and their
spectral dependences are the usual information obtained from TSL
experiments. The identity of the various defects also may be
inferred from the TSL data in some cases, but this often requires
additional information acquired from other experiments such as
optical absorption (UV-VIS-IR) or electron spin resonance (ESR).

Alpha-quartz has been the subject of numerous TSL studies
during the last three decades. These include the work of Arnold,[3]
Schlesinger,[4] Durrani et al.,[5,6] Fuller and Levy,[7] Bohm et al.,[8]
Malik et al.,[9] and Bernhardt.[10] Arnold[3] has described the quartz
TSL literature prior to 1960 and, very recently, McKeever[2] has
provided an in-depth review of the many TSL studies in quartz.
Much of the TSL work reported thus far, except for that of Malik
et al.[9] and Bernhardt,[10] has been primarily concerned with
natural quartz.

A variety of defect structures are known to exist in alpha-quartz. These include aluminum-associated trapped hole centers,[11-14] oxygen-vacancy-associated centers,[15-21] and the hydrogen atom.[22-24] From infrared absorption data, many trapping sites for OH⁻ molecules are known to exist but very few have been positively identified.[25,26] However, despite the considerable number of defect-structure studies and investigations of TSL, a satisfactory correlation of specific defects with individual TSL peaks has not been achieved in alpha-quartz.

In the present paper, we report the TSL response above room temperature from two synthetic stones and from one natural stone. Comparisons are made between the TSL obtained from swept and unswept samples cut from adjacent positions in the three stones. For each sample, data were taken with three different initial irradiation temperatures (at 77 K, at ice bath, and a double irradiation at ice bath plus 77 K) in order to make direct comparisons with the known behavior of defects in quartz, as described in previous publications from our research group.[27,28] After completion of the TSL study, the samples were subjected to an identical irradiation sequence, during which the ESR spectra of E-type centers and $[AlO_4]^0$ centers were monitored. Infrared absorption spectra provided information about the various OH⁻ centers in the samples.

Experimental Procedure

Lumbered bars of pure z-growth synthetic quartz were obtained from Sawyer Research Products, Eastlake, Ohio and from Toyo Communications Equipment Company, Japan. Also, a clear stone of Arkansas natural quartz was used. Two samples, one to be swept and the other to be left unswept, were cut from adjacent positions in each of the synthetic bars and in the natural stone. They were labeled according to the scheme introduced by Markes and Halliburton;[27] PQ for Sawyer Premium Q material, SQ for Toyo Supreme Q material, and NT for natural material. These samples had typical dimensions of 15 x 10 x 3 mm^3 in the X,Y, and Z directions, respectively.
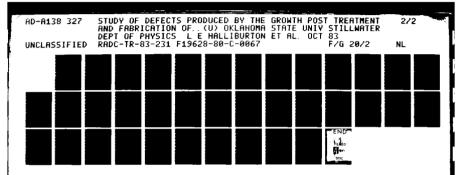
One sample from each of the three sources was swept in a hydrogen atmosphere. This sweeping was done at 400°C with an electric field of 1000 volts/cm applied along the Z axis, and the total sweeping time was 18 hrs. To sweep lithium or sodium into the quartz, the appropriate salt was deposited on one face of the crystal and an electric field of approximately 20 volts/cm was applied at 400°C for one or two hours. All electron irradiations were performed with a van de Graaff accelerator (1.7 MeV, 0.2 μA/cm^2 incident on the sample). Irradiation times were five min at 0°C and four min at 77 K. This corresponds to a dose of approximately 10^7 rads(Si) and is believed to completely saturate the TSL effects.[6] The samples were immersed directly in a water-ice mixture for the irradiations at 0°C and in liquid nitrogen for the irradiations at 77 K.
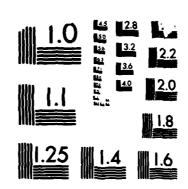
An optical cryostat with fused-quartz windows was used for

the TSL experiments, thus allowing a vacuum to be maintained around the sample during heating. The samples were mounted on a copper "cold finger" extending down from the cryostat well. The back surface of the sample was in contact with the solid copper plate. Prior to each TSL run, the sample was irradiated outside the cryostat and then mounted on the finger at room temperature. A silicone compound helped maintain thermal contact between the sample and the copper. The temperature was monitored by a copper-constantan thermocouple mounted at the bottom of the solid copper plate. A linear heating rate of 15 C^o/min was achieved by placing an immersion-type cartridge heater in the well of the cryostat.

The light emitted during heating was monitored with an EMI 9558Q photomultiplier tube (operated at 1000 volts) and a Keithley Model 601 electrometer. A high-pass optical filter, cutting off beyond 600 nm, was inserted between the sample and the phototube to minimize the response to black-body radiation. For our usual TSL runs, the full spectral output of the sample (except for the effect of the filter) was incident on the phototube, and its response was recorded on an X-Y recorder as a function of the thermocouple voltage. The spectral dependence of the emissions was determined by including a 0.5 m Bausch and Lomb monochromator in the optical detection system.

The IR spectra were taken at 80 K using a Beckman 4240 spectrophotometer and a separate optical cryostat with calcium fluoride windows. All ESR results were obtained from a homodyne spectrometer operating at X band. A Varian V-4531 rectangular

MICROCOPY RESOLUTION TEST CHART

NATIONAL BUREAU OF STANDARDS-1963-A

microwave cavity was used, and the static magnetic field was modulated at 100 kHz. The thermal anneals associated with the ESR and IR measurements were done in a small bench-top furnace. In all cases, the furnace was adjusted to the desired temperature, the sample was placed inside, and then removed after 15 min.

Results

A. Thermally Stimulated Luminescence

TSL data were obtained from six quartz crystals, representing swept and unswept samples initially cut from adjacent positions in three different stones. These results are shown in Fig. 1. Each crystal was subjected to three TSL measurements, represented by solid, dashed, and dotted curves in the six sets of data. The as-grown or as-swept sample was irradiated at 77 K and then TSL data (the solid curves) were collected as the sample was warmed from room temperature to approximately 400°C. This was followed by an irradiation at ice-bath temperature and a similar collection of data (the dashed curves) from room temperature to 400°C. The third set of TSL data (the dotted curves) from each sample was obtained over this same temperature range after the sample was given a double irradiation, first at ice-bath temperature and then at 77 K. The intensity of the TSL varied significantly from sample to sample, so the same arbitrary unit scale factor has been used for all curves to allow comparisons of peak heights from different samples and heating runs. In some cases, two of the curves in a set are referred to

90

the left ordinate scale and one curve is referred to the right ordinate scale.

The TSL data from sample PQ-G5 is shown in Fig. 1(a). This was an unswept sample of Sawyer Premium Q material, and its emission was relatively weak in the region above room temperature. However, despite the lower-intensity emission, several peaks were easily observed. After the first irradiation at 77 K, there is a prominent peak at 100°C and an additional contribution near 130°C. The ice-bath irradiation led to a quite different TSL behavior. The peak at 100°C increased in intensity by approximately a factor of two and contributions near 70°C and 130°C are larger and better resolved. Suprisingly, emission in the range 180°C to 270°C (having at least three components) increased by an order of magnitude or more. Following the ice-bath plus 77 K irradiation, the total emission decreased slightly and contributions were observed at 100°C, 130°C, 180°C, 230°C, and 270°C. In all three sets of data in Fig. 1(a) as well as in some of the other TSL traces, there is a steady increase in emission above 350°C which we attribute to "black body" radiation from the sample and holder. This effect is not observable in many of the TSL traces because of their increased range in the ordinate scale values.

The swept version of the Premium Q sample is PQ-G6 and TSL data from it are shown in Fig. 1(b). Following the initial 77 K irradiation, TSL peaks near 100°C and 140°C were found. After irradiating the sample at ice-bath temperature, the TSL peak near 100°C increased significantly and contributions near 160°C and

91

275°C appeared. After the ice-bath plus 77 K double irradiation, the TSL peaks near 100°C and 275°C were less intense and a peak near 140°C became well resolved.

SQ-B10 is an unswept sample from Toyo Supreme Q Grade material, and its TSL curves are shown in Fig. 1(c). A low-intensity peak near 90°C, possibly arising from contributions at 70°C and 100°C, along with very weak peaks near 140°C and 210°C were observed after the initial 77 K irradiation (refer to right ordinate scale). A major change again occurred after the ice-bath irradiation (now refer to left scale). The peak near 100°C increased significantly in intensity and even more intense peaks appeared near 180°C and 280°C. The TSL spectrum taken after the ice-bath plus 77 K double irradiation was nearly identical with the previous spectrum taken after an ice-bath irradiation alone. It is important to note that the intensity of the TSL peak near 280°C is very large compared to the similar peak in the Premium Q material (see Fig. 1(a)).

The swept version of the Supreme Q sample is SQ-B11 and TSL data from it are shown in Fig. 1(d). Following the initial 77 K irradiation, a weak and very broad TSL peak occurs near 115°C which possibly has contributions near 70°C, 100°C, and 130°C. After the ice-bath irradiation, the total TSL intensity increases and peaks are resolved at approximately 70°C, 100°C, and 130°C. Also, small contributions appear near 170°C and 290°C. The TSL taken after the ice-bath plus 77 K double irradiation contains a shoulder at 70°C and a larger peak at 115°C (possibly having contributions at 100°C and 130°C), and the small peak near 290°C.

The TSL data from sample NT-A1, which is unswept natural

92

material, are shown in Fig. 1(e). Peaks near 70°C and 100°C are present after the initial 7. K irradiation, along with a more intense peak near 245°C having a shoulder at 310°C (refer to right ordinate scale). As in the case of the previous two unswept samples, a significant enhancement in the TSL emission occurred after the ice-bath irradiation. The major effect in sample NT-A1 was a large increase in the peak near 245°C with contributions at 180°C, 270°C, and 310°C (now refer to left scale). The full spectral output of this latter emission was sufficiently intense to "saturate" the photomultiplier tube, and the peak information given in Fig. 1(e) was determined from a series of similar TSL runs using a monochromator. The peaks in the 70-120°C region may have increased after this second irradiation, but they are competely "overpowered" by the 180-310°C peaks. The final set of TSL data was taken on sample NT-A1 after the combined ice-bath and 77 K irradiation and it gave results similar to those obtained after the ice-bath irradiation alone.

Sample NT-A2 is the swept version of the previous sample and the TSL data from it are shown in Fig. 1(f). Following the first irradiation at 77 K, peaks are observed near 70°C, 130°C (possibly having contributions near 100°C, 130°C, and 160°C), 240°C, and 290°C (refer to right ordinate scale). After the ice-bath irradiation, peaks near 70°C, 100°C, and 130°C become more intense and better resolved (now refer to left scale). Very little change occurs in the region above 200°C. Finally, after the ice-bath plus 77 K irradiation, the TSL contains a broad peak

93

near 125°C which probably contains contributions at 100°C and 130°C.

The spectral dependence of the 280°C peak present after the ice-bath plus 77 K irradiation of sample SQ-B10 (dotted curve in Fig. 1(c)) is shown in Fig. 2. These data have been corrected for the variation in response of the detection system (i.e., photomultiplier tube and monochromator). The spectral dependence of the emission for this peak rises to a maximum near 465 nm with a less rapid decrease on the low energy side. Similar spectral dependences were found for the 180°C peak in this sample and for the 245°C peak in the natural sample. Spectral dependence data were not obtained from sample PQ-G5 or PQ-G6 because of their low-intensity emissions. It should be noted that our results are in direct agreement with the spectral dependence determined in previous studies.[6]

A final set of TSL experiments were done on two SQ-A samples, one lithium-swept and the other sodium-swept. These electrodiffusion treatments left only lithium or sodium, respectively, in the crystals and allowed us to determine if any features in the TSL could be correlated with a specific interstitial alkali ion. Following an ice-bath irradiation, the resulting TSL from both of the alkali-swept samples appeared similar to the corresponding data from the unswept sample SQ-B10 (shown by the dashed curve in Fig. 1(c)). No significant differences in the TSL were found in the 200°C to 300°C region for the Li and Na-swept samples when data were obtained under nearly identical conditions. The peak temperatures agreed within approximately 10 C°, and the intensities were comparable (with

94

the Li-swept sample giving 2-3 times more emission than the Na-swept sample).

B. Electron Spin Resonance

After obtaining the TSL data, the six quartz samples were returned to their as-grown or as-swept condition by annealing at $500^{\circ}C$ for 5 hrs. Then, the samples were subjected to the same sequence of irradiations and thermal anneals as in the TSL experiments, and the ESR spectra were monitored at room temperature preceding each anneal. These latter spectra revealed the intensity of the E_2' and E_4' centers,[18,19] which are $S = 1/2$, $I = 1/2$ defects, and the E_1'', E_2'', and E_3'' centers,[20] which are $S = 1$ defects. When the sample reached $300^{\circ}C$ during each anneal, it was returned to room temperature where the intensity of the E_1' center[21] was monitored, and then the sample was heated to $400^{\circ}C$ to complete the particular anneal. The ESR results for these E-type centers are given in Table I. Because of severe microwave power saturation effects, no measurements of the absolute E-type center concentrations were made and only relative values are given in the table.

Smaller samples ($7 \times 2 \times 3$ mm^3 in the X, Y, and Z directions, respectively) for use in monitoring the concentrations of $[AlO_4]^{\circ}$ centers[12] were cut from the center of each plate after the preceding TSL and ESR experiments were completed. The smaller size was required to allow the samples to fit into the "finger" Dewar used for the 77 K ESR measurements. This

cutting process also provided samples that were used in the infrared absorption measurements described in Section III C.

These smaller ESR samples were subjected to the same sequence of irradiations and thermal anneals as the earlier set of samples. After each of the two irradiations at 77 K, the intensity of the $[AlO_4]^O$ center ESR spectrum was monitored at 77 K without sample warmup. Next, following all three initial irradiations, the samples were held briefly at room temperature and then cooled to 77 K where the $[AlO_4]^O$ centers were again monitored. After this, the samples were heated to 200^OC, then cooled to 77 K and the $[AlO_4]^O$ centers were once again monitored. A measurement of the absolute aluminum content was made for sample SQ-B10 (following the ice-bath plus 77 K irradiations and without subsequent warming) by comparing to an $Al_2O_3:Cr^{3+}$ standard sample obtained from the National Bureau of Standards. This calibrated the $[AlO_4]^O$ center ESR spectra from the various samples, and the entire set of data is presented in Table II. The aluminum content of each sample is equal to the number of $[AlO_4]^O$ centers present after the ice-bath plus 77 K irradiations.[27] *The effectiveness of the sweeping (i.e.,* percentage of interstitial alkali ions removed by sweeping) is given by the ratio of $[AlO_4]^O$ centers present at 77 K after the initial 77-K irradiation to those present at 77 K after the ice-bath plus 77 K irradiations.[27] In the case of the unswept samples, *the aluminum content, relative to Si, is 12.3 ppm, 13.7* ppm, and 80.5 ppm for PQ-G5, SQ-B10, and NT-A1, respectively. The aluminum content is 7.6 ppm, 6.0 ppm, and 65.7 ppm and the effectiveness of sweeping is 91.6, 95.6, and 88.2 per cent for

the PQ-G6, SQ-B11, and NT-A2 samples, respectively.

A careful comparison of the thermal decay behavior of the $[AlO_4]^O$ centers was made for the unswept samples SQ-B10 and NT-A1. These samples were subjected to a pulsed anneal sequence above room temperature after an ice-bath plus 77 K irradiation. They were held simultaneously for 15-min periods at an elevated temperature and then their $[AlO_4]^O$ center ESR spectrum was monitored at 77 K before proceeding to the next anneal temperature. It was found that the decay curves for the $[AlO_4]^O$ centers were displaced relative to each other by approximately 25 C^O, although they were otherwise similar in the two samples. The temperature at which half the centers had decayed in the SQ-B10 sample was greater than the equivalent temperature for sample NT-A1. This result implies that the TSL peaks at $280^O C$ in sample SQ-B10 and at $245^O C$ in sample NT-A1 are probably associated with the same phenomenon.

C. Infrared Absorption

A set of smaller samples for infrared measurements were cut from the original unswept plates at the same time the previously described set of samples for the 77 K ESR measurements were obtained. These infrared samples are approximately 5 x 10 x 3 mm^3 in the X, Y, and Z directions, respectively. Infrared absorption data, taken at 80 K in the 3100 to 3600 cm^{-1} region, are shown in Fig. 3 for the three unswept samples. Prior to these measurements, each of the samples had been annealed near $500^O C$

97

for six hours to restore them to their as-grown condition.

The two broad bands at 3200 and 3300 cm^{-1} in Fig. 3 are common to all three samples and are attributed to intrinsic Si-O lattice vibrations. They do not depend on impurities or other defects in the crystal and provide a built-in calibration of the absorption scale. There are additional bands in Fig. 3 which are due to OH$^-$ defects trapped adjacent to imperfections in the quartz. Figure 3(a) is from sample NT-A1 and contains two bands, at 3306 and 3367 cm^{-1}, which have been assigned[26,28] to the Al-OH$^-$ center (i.e., an OH$^-$ molecule trapped adjacent to a substitutional aluminum ion). ·A very small amount of these two bands can be discerned in Fig. 3(b), which is from sample SQ-B10, and no contribution to these two bands can be found in Fig. 3(c), which is from sample PQ-G5.

The presence of the three bands at 3400, 3440, and 3585 cm^{-1} in sample PQ-G5, as shown in Fig. 3(c), is considered to be important. These three bands[29] are essentially absent from sample SQ-B10 and they are small, but observable, in sample NT-A1. Koumvakalis and Markes[30] have shown that these latter three bands are OH$^-$-related and Martin and Armington[31] have shown that their presence correlates with faster crystal growth rates for synthetic quartz.

Discussion

Our study has included two synthetic stones and one natural stone, and has allowed comparison of swept and unswept samples cut from adjacent positions in each of these stones. Although

the temperatures corresponding to the TSL peaks varied slightly from sample to sample, a pattern emerged in which emissions were found near 60-70°C, near 100°C, near 120-130°C, near 180°C, near 230-245°C, and near 270-280°C.

The most interesting of the observed TSL emissions are in the 200°C to 300°C region. Among the striking features of these latter emissions are their absence in all samples receiving only an initial 77 K irradiation, their presence in all unswept samples following both the ice-bath and ice-bath plus 77 K irradiations, and their absence in the swept samples following both the ice-bath and ice-bath plus 77 K irradiations. Sample NT-A1, the unswept natural specimen, must be considered a special case since it has presumably accumulated a certain environmental radiation dose at temperatures well above 77 K during its geologic history. More simply stated, our observations indicate that the 200-300°C emissions are not prominent whenever the interstitial alkali ions are either located adjacent to the substitutional aluminum ions, as is the situation following the initial 77 K irradiation alone, or are removed from the crystal, as is the case for the swept samples. This correlation with the behavior of alkali ions is supported by previous investigations[27,28] that show alkali ions remain associated with aluminum until the crystal is irradiated above 200 K and that show hydrogen sweeping removes the alkalis from the crystal.

Additional evidence suggests the interstitial alkali ions play an important role in the higher-temperature TSL response. In quartz that is free of germanium or other impurities except

99

aluminum, hydrogen, and alkalis, the only condition during which
$[AlO_4]^0$ centers can be created is when the alkali ions are away
from the aluminum sites.[27,28] This situation is best explained
by assuming that the removed alkali ions act as electron traps, a
role they can not fulfill when they remain next to the aluminum
ions. Separate experiments have shown that a thermally induced
return of the interstitial alkali to the aluminum site, after
having been removed by irradiation at lower temperature,
coincides with the thermal anneal of the $[AlO_4]^0$ centers.[32] It
has previously been shown by Jani et al.[21] and again in the
present study that the $[AlO_4]^0$ centers undergo a significant
thermal anneal step in the region 200 to 300°C. This is the
final anneal step for the $[AlO_4]^0$ centers, i.e., none remain
after heating above 300°C.

Since the $[AlO_4]^0$ centers are the only known holelike
centers in quartz having a major decay step between 200 and
300°C, they are expected to participate in the TSL processes in
this temperature range. This is also suggested by the results in
Table II. Comparing the relative numbers of $[AlO_4]^0$ centers
present after the 200°C anneals shows that only unswept samples,
following either ice-bath or ice-bath plus 77 K irradiations,
have large concentrations of $[AlO_4]^0$ centers available for
recombination, and it is exactly these conditions which lead to
intense TSL peaks in the 200-300°C region.

Assuming that the $[AlO_4]^0$ centers are involved in the TSL,
the question then becomes whether the recombination occurs at the
electron trapping site or at the $[AlO_4]^0$ center. In our present
investigation, we have found that the final anneal step of the

$[AlO_4]^o$ centers can occur at measurably different temperatures in different samples (e.g., near 250°C in sample NT-A1 and near 275°C in sample SQ-B10). These anneal temperatures coincide reasonably well with the temperatures of the maximum emission from the same samples in the 200-300°C range. This suggests that electrons are being released from their traps and are recombining with the hole at the $[AlO_4]^o$ center. If holes were being released from $[AlO_4]^o$ centers and recombining with electrons at the electrons' trapping sites, only one TSL peak would be observed in the 200-300°C region because the $[AlO_4]^o$ centers could have only one characteristic temperature for release of the hole. The conclusion that both the 245°C and 280°C TSL peaks are due to electrons recombining with the hole at the $[AlO_4]^o$ centers is further supported by the similar spectral dependence of the emission peaks.

The alkali ions present in our samples can be either Li^+ or Na^+ or a combination of the two, and the possibility arises that the 245°C and 280°C TSL peaks are associated with the release of electrons from traps involving different types of alkali ions. However, when two samples from the same quartz bar were separately swept with lithium and sodium, no significant differences were found in the subsequent TSL experiments. This indicates that there is not a single type of trapping site for the electron which has two different decay temperatures (i.e., 245° and 280°C) depending on which alkali ion is present. Instead, we suggest there must be two or more distinct trapping sites for the electrons. One of these trapping sites dominates

101

in the NT-A samples and a different trapping site dominates in the SQ-B samples. The existence of different electron trapping sites in the two samples is supported indirectly by the significant differences in the infrared absorption data shown in Fig. 3 for the two samples. Although the TSL peak intensities in the 200-300°C range are lower in the PQ-G sample, it too appears to have both types of trapping sites present (see Fig. 1(a)).

Finally, consider the TSL peaks below 200°. There are good correlations of the TSL peak temperatures in this range with the known thermal decay temperatures of various ESR spectra. Specifically, the E_2'' centers decay near 50°C, the E_1' and E_3'' centers around 90°C, and E_2' and E_4' centers near 180°C. However, no direct correlation is found when comparing the intensities of the TSL peaks at these temperatures with the relative intensities of the E-centers given in Table I. This suggests that additional unobserved defects are participating in the recombination processes. An important feature of these TSL peaks below 200°C is their presence, with similar intensities, in both hydrogen swept and unswept samples. This suggests that these peaks are in some way associated with hydrogen. An increase in the Al-OH$^-$ centers[33] and a corresponding decrease in the $[AlO_4]^0$ centers have been previously observed near 100°C. Also, Table II shows that there is a decrease in $[AlO_4]^0$ centers between room temperature and 200°C in our present series of samples.

Summary

A large number of TSL peaks have been observed in both synthetic and natural quartz in the above-room-temperature

102

region. These peaks are divided into two categories, below and above 200°C. The first category contains a number of peaks in the 60°C to 130°C range as well as a peak near 180°C. As a result of previous investigations, E'' centers are known to decay in the 60°C to 100°C region and E_2' and E_4' centers are known to decay at 180°C. Careful comparison of TSL and ESR data from the present study have shown that there is no simple and direct correlation between the intensities of these TSL peaks and the E-type centers, although there must be an indirect association via additional unobserved defects. Because the TSL peaks in the 60° to 130°C region were similar in hydrogen-swept and unswept samples taken from the same stone, we suggest that these peaks are associated with hydrogen.

The TSL peaks above 200°C, specifically at 245°C or 280°C depending on the sample, are found only in unswept samples that have received a radiation dose while near room temperature. This has been interpreted to mean that interstitial alkali ions are involved in the TSL process above 200°C; the reasons being that alkali ions are not removed from aluminum sites unless the crystal has been irradiated above 200 K and that hydrogen sweeping replaces all alkali ions with hydrogen. Spectral dependences for these two above-200°C peaks are identical, and the $[AlO_4]^O$-center decay corresponds well with the position of these TSL peaks in each sample. Our observations suggest that the recombination is taking place at the same site, namely the $[AlO_4]^O$ center. There must then be at least two electron trapping sites, having different decay temperatures, and which we believe have associated alkali ions.

103

References

1. P. Braunlich, P. Kelly, and J. -P. Fillard, in <u>Thermally</u> <u>Stimulated</u> <u>Relaxation</u> <u>in</u> <u>Solids</u>, edited by P. Braunlich (Springer-Verlag, Berlin, 1979), Chap. 2, pp. 35-92; L. A. DeWerd, <u>ibid</u>, Chap. 6, pp. 275-299.

2. S. W. S. McKeever, Radiation Protection Dosimetry (in press).

3. G. W. Arnold, Jr., J. Phys. Chem. Solids 13, 306 (1960).

4. M. Schlesinger, Phys. Lett. 10, 49 (1964).

5. S. A. Durrani, P. J. Groom, K. A. R. Khazal, and S. W. S. McKeever, J. Phys. D 10, 1351 (1977).

6. S. A. Durrani, K. A. R. Khazal, S. W. S. McKeever, and R. J. Riley, Radiat. Eff. 33, 237 (1977).

7. G. E. Fuller and P. W. Levy, presented at the International Conference on Defects in Insulating Crystals, Gatlinburg, Tennessee, October 9-14, 1977 (see Conference Abstracts, pp. 142-3).

8. M. Bohm, W. Peschke, and A. Scharmann, Radiat. Eff. 53, 67 (1980).

9. D. M. Malik, E. E. Kohnke, and W. A. Sibley, J. Appl. Phys. 52, 3600 (1981).

10. Hj. Bernhardt, Phys. Stat. Sol. (a) 74, 159 (1982).

11. J. A. Weil, Radiat. Eff. 26, 261 (1975).

12. R. H. D. Nuttall and J. A. Weil, Can. J. Phys. 59, 1696 (1981).

13. R. H. D. Nuttall and J. A. Weil, Can. J. Phys. 59, 1709 (1981).

14. R. H. D. Nuttall and J. A. Weil, Can. J. Phys. 59, 1886 (1981).

15. R. A. Weeks, J. Appl. Phys. 27, 1376 (1956).

16. R. H. Silsbee, J. Appl. Phys. 32, 1459 (1961).

17. R. A. Weeks and C. M. Nelson, J. Am. Ceram. Soc. $\underline{43}$, 399 (1960).

18. R. A. Weeks, Phys. Rev. $\underline{130}$, 570 (1963).

19. J. Isoya, J. A. Weil, and L. E. Halliburton, J. Chem. Phys. $\underline{74}$, 5436 (1981).

20. R. B. Bossoli, M. G. Jani, and L. E. Halliburton, Solid State Commun. $\underline{44}$, 213 (1982).

21. M. G. Jani, R. B. Bossoli, and L. E. Halliburton, Phys. Rev. B $\underline{27}$, 2285 (1983).

22. R. A. Weeks and M. Abraham, J. Chem. Phys. $\underline{42}$, 68 (1965).

23. B. D. Perlson and J. A. Weil, J. Magn. Res. $\underline{15}$, 594 (1974).

24. J. Isoya, J. A. Weil, and P. H. Davis, J. Phys. Chem. Solids, $\underline{44}$, 335 (1983).

25. A. Kats, Philips Res. Rep. $\underline{17}$, 133 (1962).

26. R. N. Brown and A. Kahan, J. Phys. Chem. Solids $\underline{36}$, 467 (1975).

27. M. E. Markes and L. E. Halliburton, J. Appl. Phys. $\underline{50}$, 8172 (1979).

28. L. E. Halliburton, N. Koumvakalis, M. E. Markes, and J. J. Martin, J. Appl. Phys. $\underline{52}$, 3565 (1981).

29. H. G. Lipson, F. Euler, and P. A. Ligor, Proceedings of the 33rd Annual Symposium on Frequency Control (1979), p. 122.

30. N. Koumvakalis and M. Markes, J. Appl. Phys. $\underline{51}$, 3431 (1980).

31. J. J. Martin and A. F. Armington, J. Cryst. Growth $\underline{62}$, 203 (1983).

32. J. J. Martin (private communication).

33. B. Subramaniam (private communication).

Table I. Relative concentrations of the E-type centers following the three different initial irradiations. An arbitrary set of units is used.
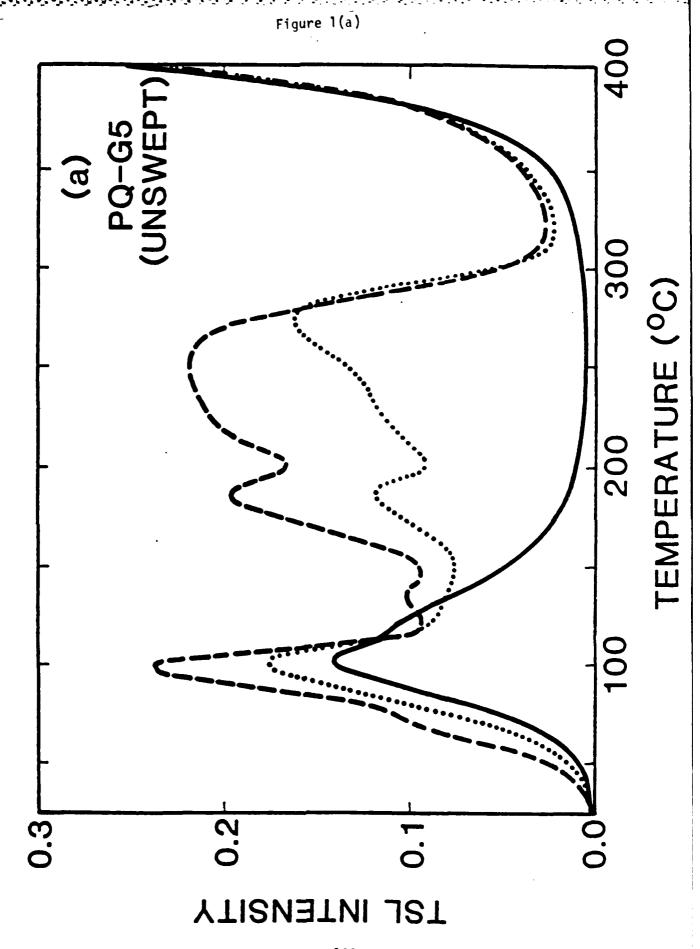
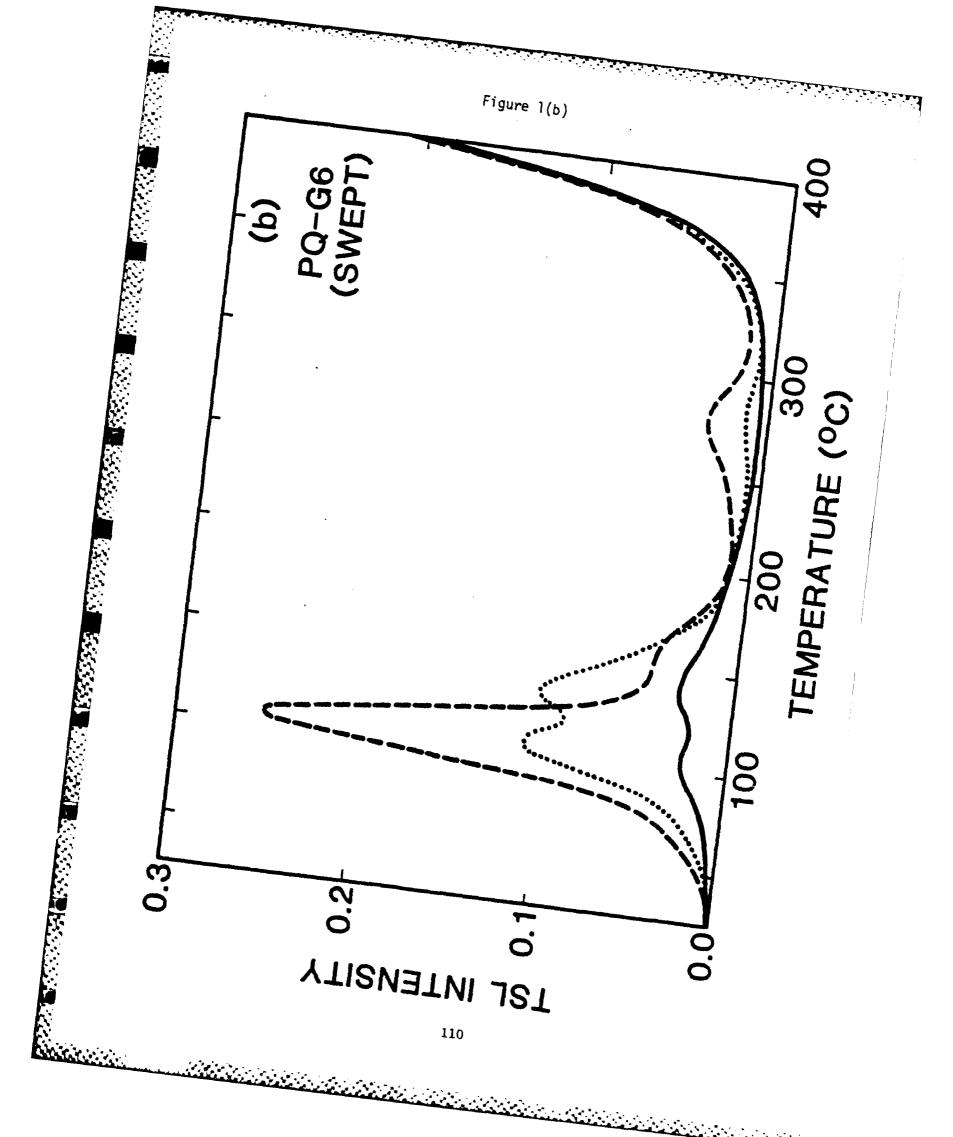| Center	Initial 77 K Irradiation		Ice-bath Irradiation		Ice-bath plus 77 K Irradiation	
	PQ-G5 (unswept)	PQ-G6 (swept)	PQ-G5 (unswept)	PQ-G6 (swept)	PQ-G5 (unswept)	PQ-G6 (swept)
E_1''	0	0	0	0	68	45
E_2''	0	0	0	0	23	13
E_3''	0	0	0	0	13	9
E_2'	5.8	6.2	56	63	20	15
E_4'	1.4	2	18	18	23	32
E_1'	0	0	16	74	20	39
	SQ-B10 (unswept)	SQ-B11 (swept)	SQ-B10 (unswept)	SQ-B11 (swept)	SQ-B10 (unswept)	SQ-B11 (swept)
E_1''	13.5	0	4.5	0	106	22.5
E_2''	5.2	0	18	0	38	8
E_3''	5.2	0	0	0	28	5.5
E_2'	7.5	1.9	26.5	48.5	-	-
E_4'	6	0.9	9.5	13	11	30
E_1'	10	3.2	53	22.5	76	29
	NT-A1 (unswept)	NT-A2 (swept)	NT-A1 (unswept)	NT-A2 (swept)	NT-A1 (unswept)	NT-A2 (swept)
E_1''	0	0	0	0	46	0
E_2''	0	0	0	0	19	0
E_3''	0	0	0	0	12.5	0
E_2'	10	2.1	27	45	-	10.8
E_4'	23	2.2	11.5	18	27.5	18
E_1'	52	10.6	124	8.8	212	20.8

Table II. $[AlO_4]^o$ center concentration at various annealing stages following each of the different initial irradiations. The defect concentrations are given in units of 10^{16} cm^{-3}. [1 ppm(Si) = 2.65 x 10^{16} cm^{-3}]
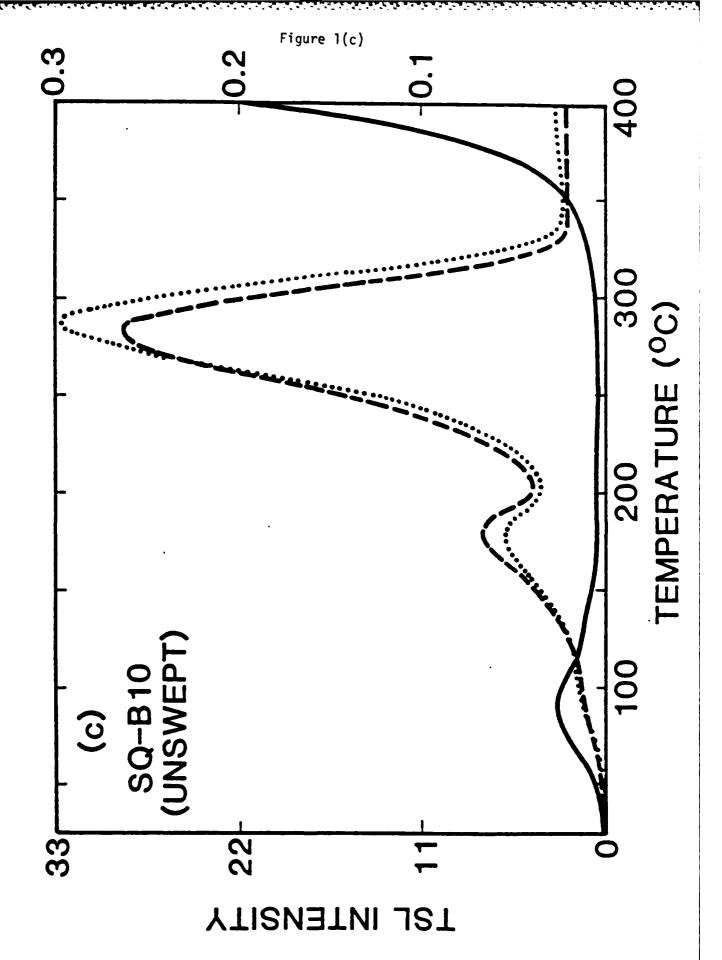
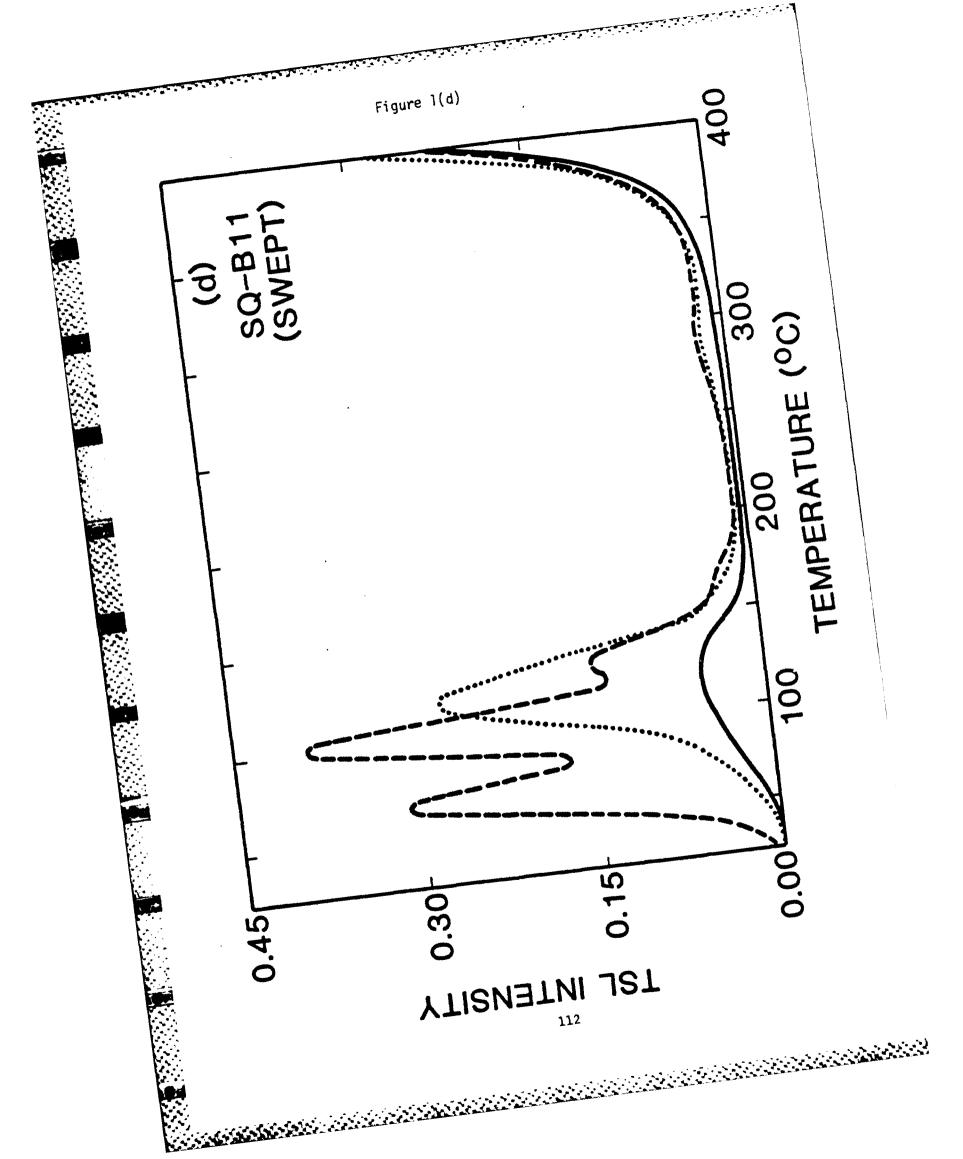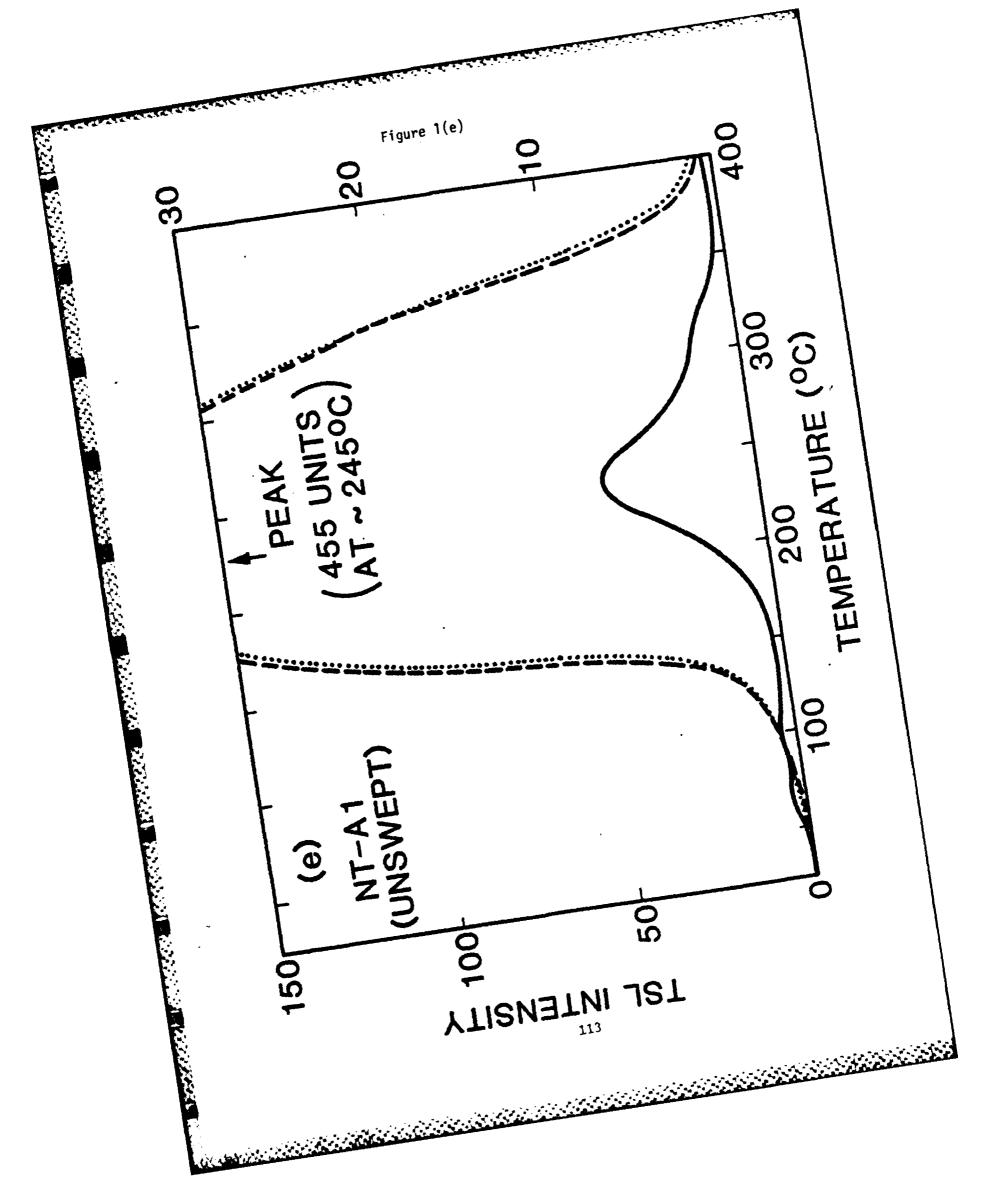|	Initial 77 K Irradiation		Ice-bath Irradiation		Ice-bath plus 77 K Irradiation	
	PQ-G5 (unswept)	PQ-G6 (swept)	PQ-G5 (unswept)	PQ-G6 (swept)	PQ-G5 (unswept)	PQ-G6 (swept)
Before warming	0.9	18.5	-	-	32.6	20.2
After RT anneal	0	2.6	6.9	5.5	10.2	4.3
After 200°C anneal	0	0	2.7	2.4	3.8	0.6
	SQ-B10 (unswept)	SQ-B11 (swept)	SQ-B10 (unswept)	SQ-B11 (swept)	SQ-B10 (unswept)	SQ-B11 (swept)
Before warming	5.5	15.2	-	-	36.3	15.9
After RT anneal	2.6	1.8	29.9	2.5	34.4	3.8
After 200°C anneal	1.8	0	22.4	1.1	23.9	1.3
	NT-A1 (unswept)	NT-A2 (swept)	NT-A1 (unswept)	NT-A2 (swept)	NT-A1 (unswept)	NT-A2 (swept)
Before warming	20.6	153.4	-	-	213.3	174.0
After RT anneal	8.9	15.0	202.1	9.9	196.5	47.9
After 200°C anneal	4.5	1.0	67.4	4.7	74.8	6.5

Figure Captions

1. TSL spectra from the three unswept and three swept quartz samples. The solid curves were taken after irradiation at 77 K, the dashed curves were taken after irradiation at ice-bath temperature, and the dotted curves were taken after irradiation at ice bath plus 77 K. In (c), (e), and (f), the solid curves are referred to the right ordinate scales. The same arbitrary unit scale factor for TSL intensity has been used for all six sets of data.

2. Spectral dependence of the 280°C TSL peak occurring in sample SQ-B10 after an ice-bath plus 77 K irradiation. The data have been corrected for variations in the detection system response.

3. Infrared absorption spectra taken at 80 K after annealing near 500°C (i.e., restoring to the as-grown condition). The unpolarized light propagated parallel to the c axis. Trace (a) is from the sample NT-A1, trace (b) is from sample SQ-B10, and trace (c) is from sample PQ-G5.

Figure 1(a)

(a)
PQ-G5
(UNSWEPT)

Figure 1(b)

PQ-G6
(SWEPT)
(b)

TSL INTENSITY

TEMPERATURE (°C)

110

Figure 1(c)

Figure 1(c)

(c)
SQ-B10
(UNSWEPT)

TSL INTENSITY

TEMPERATURE (°C)

Figure 1(d)

(d)
SQ-B11
(SWEPT)

TSL INTENSITY

TEMPERATURE (°C)

112

Figure 1(e)

(e) NT-A1 (UNSWEPT)

PEAK
(455 UNITS
AT ~245°C)

TEMPERATURE (°C)

TSL INTENSITY

113

Figure 1(f)

(f)
NT-A2
(SWEPT)

TEMPERATURE (°C)

TSL INTENSITY

114
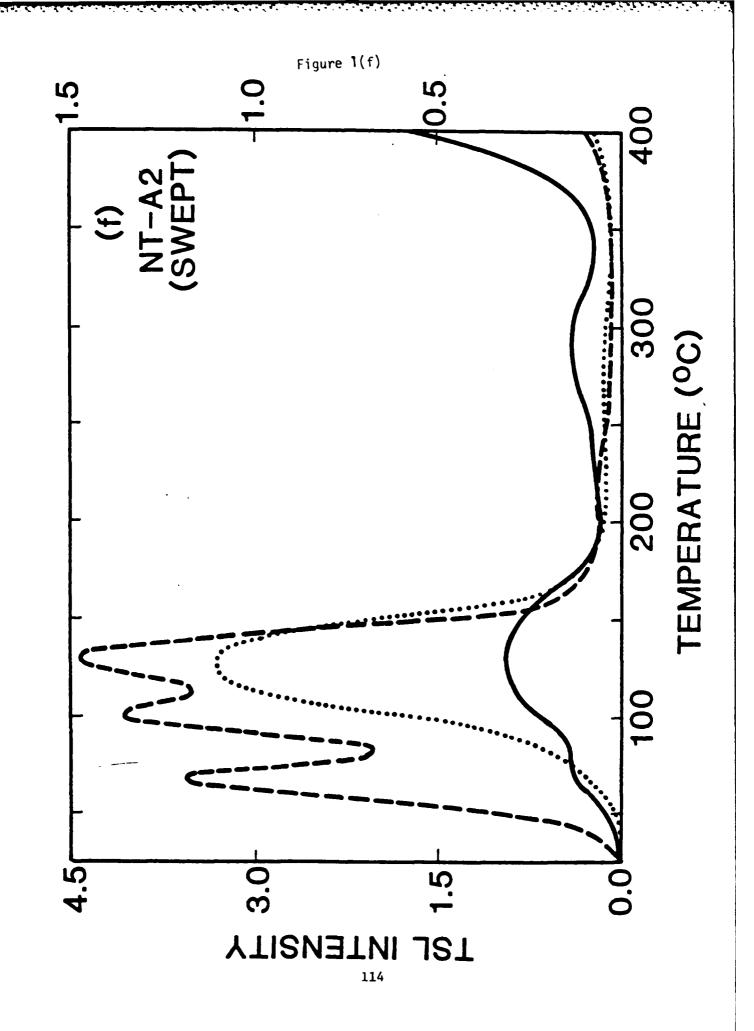
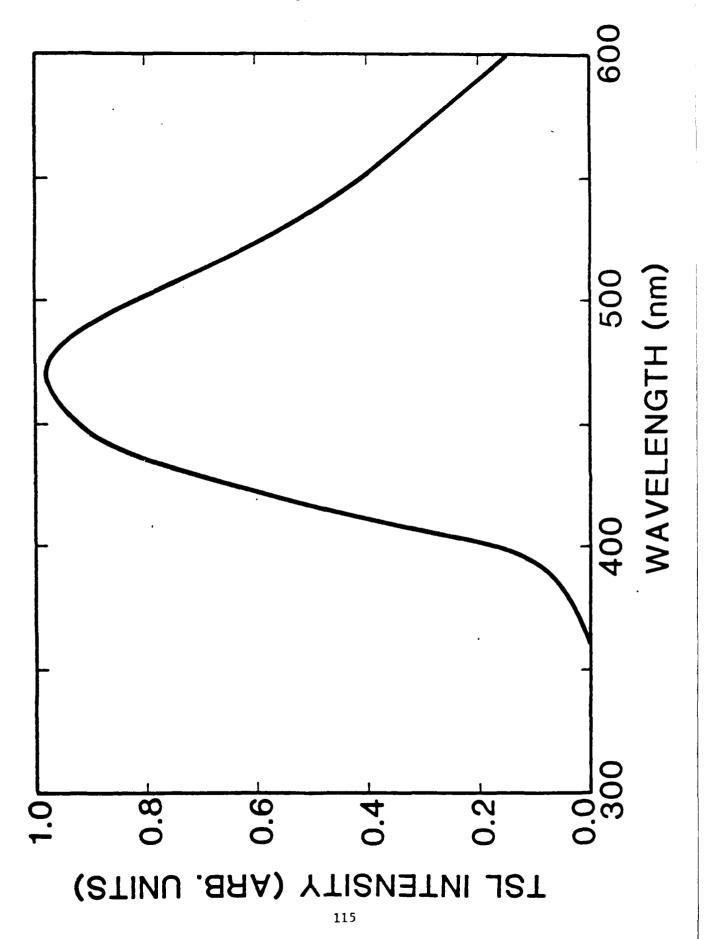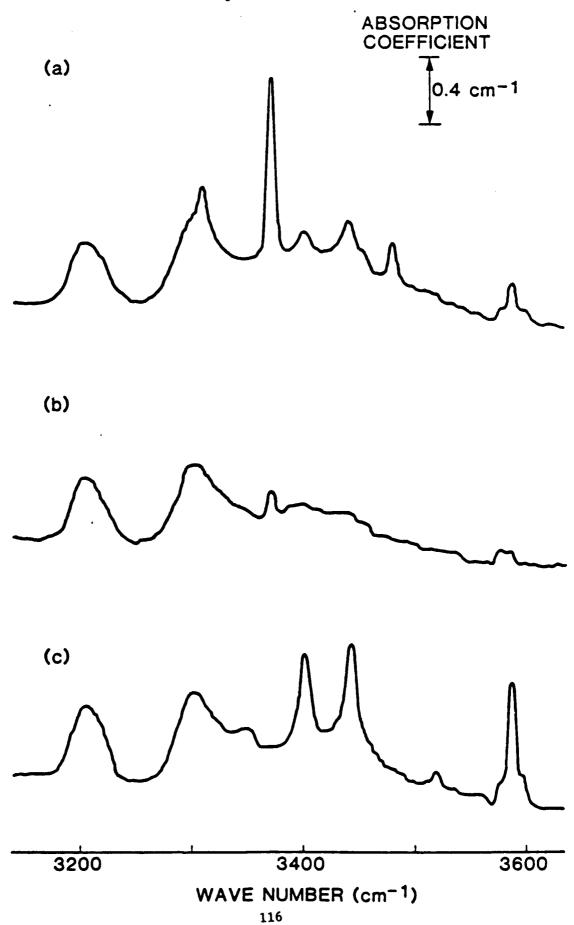Figure 2

115

Figure 3

116

VIII. EVALUATION OF RADC-GROWN QUARTZ

Recently, the Air Force has established a Hydrothermal Growth Facility at Rome Air Development Center (RADC), Hanscom AFB. As part of our contract, we performed evaluation tests for aluminum content in the quartz grown by the Air Force at this facility. The aluminum is a pervasive and active impurity in all quartz, and its concentration is a good indicator of the quality of a quartz bar. The aluminum content was measured by the electron spin resonance (ESR) technique, as described by Markes and Halliburton [J. Appl. Phys. $\underline{50}$, 8172 (1979)]. Table I summarizes these aluminum determinations.

Table I. Summary of aluminum analyses of RADC-grown quartz.

Sample	Al content (ppm)
X7-1 (X growth)	21.0
X7-1 (Z growth)	4.6
X7-2 (Z growth)	11.0
X7-3 (Z growth)	4.6
X7-4 (Z growth)	9.0
X23 (seed)	2.0
X23	967.0
X33	7.1
F2	12.4
QA4-P (Boule 1)	16.4

QA4-U (Boule 2)	19.8
QA5-B	0.9
QA6	0.8
QA7	1.7
QA8-B	0.9
QA8-T	0.7
QA9 (Large Boule)	9.4
QA9 (Small Boule)	1.3
QA10 (Large Boule)	1.8
QA10 (Small Boule)	3.5

IX. LIST OF PAPERS, PRESENTATIONS, AND THESES

The following papers, presentations, and theses resulted from the research performed at Oklahoma State University under this contract.

Papers (in refereed journals)

L. E. Halliburton, N. Koumvakalis, M. E. Markes, and J. J. Martin, RADIATION EFFECTS IN CRYSTALLINE SiO_2: THE ROLE OF ALUMINUM, J. Appl. Phys. <u>52</u>, 3565 (1981).

M. Jalilian-Nosraty and J. J. Martin, THE EFFECTS OF IRRADIATION AND ELECTROLYSIS ON THE THERMAL CONDUCTIVITY OF SYNTHETIC QUARTZ, J. Appl. Phys. <u>52</u>, 785 (1981).

J. Isoya, J. A. Weil, and L. E. Halliburton, EPR AND AB INITIO SCF-MO STUDIES OF THE Si·H-Si SYSTEM IN THE E_4' CENTER OF α-QUARTZ, J. Chem. Phys. <u>74</u>, 5436 (1981).

D. M. Malik, E. E. Kohnke, and W. A. Sibley, LOW-TEMPERATURE THERMALLY STIMULATED LUMINESCENCE OF HIGH QUALITY QUARTZ, J. Appl. Phys. <u>52</u>, 3600 (1981).

R. B. Bossoli, M. G. Jani, and L. E. Halliburton, RADIATION-INDUCED E'' CENTERS IN CRYSTALLINE SiO_2, Solid State Commun. <u>44</u>, 213 (1982).

J. J. Martin and A. F. Armington, EFFECT OF GROWTH RATE ON QUARTZ DEFECTS, J. Cryst. Growth <u>62</u>, 203 (1983).

M. G. Jani, R. B. Bossoli, and L. E. Halliburton, FURTHER CHARACTERIZATION OF THE E_1' CENTER IN CRYSTALLINE SiO_2, Phys. Rev. B <u>27</u>, 2285 (1983).

P. J. Alonso, L. E. Halliburton, E. E. Kohnke, and R. B. Bossoli, X-RAY-INDUCED LUMINESCENCE IN CRYSTALLINE SiO_2, J. Appl. Phys. (in press).

K. B. Hitt and J. J. Martin, RADIATION-INDUCED MOBILITY OF LITHIUM AND SODIUM IN ALPHA-QUARTZ, J. Appl. Phys. (in press).

M. G. Jani, L. E. Halliburton, and E. E. Kohnke, POINT DEFECTS IN CRYSTALLINE SiO_2: THERMALLY STIMULATED LUMINESCENCE ABOVE ROOM TEMPERATURE, J. Appl. Phys. (in press).

R. B. Bossoli and L. E. Halliburton, ^{27}AL HYPERFINE AND QUADRUPOLE INTERACTIONS FOR THE $[AlO_4]^O$ CENTER IN QUARTZ, submitted to Phys. Rev. B.

Conference Proceedings

J. J. Martin, L. E. Halliburton, and R. B. Bossoli, POINT DEFECTS IN CULTURED QUARTZ: RECENT ACOUSTIC LOSS, INFRARED, AND MAGNETIC RESONANCE RESULTS, Proceedings of the 35th Annual Symposium on Frequency Control (1981), p. 317.

J. J. Martin, L. E. Halliburton, R. B. Bossoli, and A. F. Armington, THE INFLUENCE OF CRYSTAL GROWTH RATE AND ELECTRODIFFUSION (SWEEPING) ON POINT DEFECTS IN ALPHA-QUARTZ, Proceedings of the 36th Annual Symposium on Frequency Control (1982), p. 77.

J. J. Martin, R. B. Bossoli, L. E. Halliburton, B. Subramaniam, and D. West, ELECTRODIFFUSION OF CHARGE-COMPENSATING IONS IN ALPHA-QUARTZ, Proceedings of the 37th Annual Symposium on Frequency Control (1983), (in press).

J. J. Martin, THERMAL- AND RADIATION-INDUCED MOBILITIES OF CHARGE COMPENSATION IONS IN CRYSTALLINE SiO_2, Proceedings of the 4th Europhysical Topical Conference on Lattice Defects in Ionic Crystals (1982), (in press).

L. E. Halliburton, M. G. Jani, and R. B. Bossoli, ELECTRON SPIN RESONANCE AND OPTICAL STUDIES OF OXYGEN VACANCY CENTERS IN QUARTZ, Proceedings of the 2nd International Conference on Radiation Effects in Insulators, (1983), (in press).

Presentations (at APS-March Meetings)

J. J. Martin and A. Jafari, ALUMINUM-HOLE CENTER RELATED ACOUSTIC LOSS IN AT-CUT QUARTZ, Bull. Am. Phys. Soc. 26, 235 (1981).

R. B. Bossoli and L. E. Halliburton, ELECTRON SPIN RESONANCE OF E-TYPE CENTERS IN ALPHA-QUARTZ, Bull. Am. Phys. Soc. 26, 236 (1981).

J. D. Howe, L. A. Kappers, L. E. Halliburton, and A. F. Armington, ESR STUDY OF A RADIATION-INDUCED DEFECT IN $AlPO_4$, Bull. Am. Phys. Soc. 26, 235 (1981).

E. E. Kohnke, D. M. Malik, and W. A. Sibley, LOW TEMPERATURE THERMOLUMINESCENCE OF QUARTZ, Bull. Am. Phys. Soc. 26, 235 (1981).

K. B. Hitt, M. Mayer, and J. J. Martin, RADIATION-INDUCED MOBILITY OF ALKALI IONS IN ALPHA-QUARTZ, Bull. Am. Phys. Soc. 27, 257 (1982).

J. J. Martin, L. E. Halliburton, and A. F. Armington, CRYSTAL GROWTH RATE DEPENDENCE OF OH-RELATED DEFECTS IN SYNTHETIC QUARTZ, Bull. Am. Phys. Soc. 27, 257 (1982).

M. G. Jani, R. B. Bossoli, and L. E. Halliburton, ESR STUDY OF THE E″ CENTERS IN ALPHA-QUARTZ, Bull. Am. Phys. Soc. 27, 257 (1982).

R. B. Bossoli, J. J. Martin, and L. E. Halliburton, ELECTRODIFFUSION IN CRYSTALLINE SiO_2, Bull. Am. Phys. Soc. 27, 256 (1982).

L. E. Halliburton, P. J. Alonso, E. E. Kohnke, and R. B. Bossoli, X-RAY-INDUCED LUMINESCENCE IN CRYSTALLINE SiO_2, Bull. Am. Phys. Soc. <u>27</u>, 256 (1982).

J. J. Martin, HIGH TEMPERATURE ANNEALING BEHAVIOR OF ALUMINUM-RELATED CENTERS IN ALPHA-QUARTZ, Bull. Am. Phys. Soc. <u>28</u>, 494 (1983).

M. G. Jani, R. B. Bossoli, and L. E. Halliburton, ESR STUDY OF THE E_1' CENTER IN CRYSTALLINE SiO_2, Bull. Am. Phys. Soc. <u>28</u>, 494 (1983).

E. E. Kohnke, M. G. Jani, and L. E. Halliburton, THERMOLUMINESCENCE OF CRYSTALLINE SiO_2, Bull. Am. Phys. Soc. <u>28</u>, 494 (1983).

Theses (at Oklahoma State University)

K. B. Hitt, RADIATION-INDUCED MOBILITY OF ALKALI-ELECTROLIZED SYNTHETIC QUARTZ, M.S., July, 1982.

S. P. Doherty, RADIATION EFFECTS IN QUARTZ RESONATORS, Ph.D., May, 1980.

M. G. Jani, RADIATION EFFECTS IN CRYSTALLINE SiO_2: STRUCTURE OF THE E'' CENTERS, Ph.D., May, 1982.

MISSION
of
Rome Air Development Center

RADC plans and executes research, development, test and selected acquisition programs in support of Command, Control Communications and Intelligence (C^3I) activities. Technical and engineering support within areas of technical competence is provided to ESD Program Offices (POs) and other ESD elements. The principal technical mission areas are communications, electromagnetic guidance and control, surveillance of ground and aerospace objects, intelligence data collection and handling, information system technology, ionospheric propagation, solid state sciences, microwave physics and electronic reliability, maintainability and compatibility.

MISSION
of
Rome Air Development Center

RADC plans and executes research, development, test and selected acquisition programs in support of Command, Control Communications and Intelligence (C³I) activities. Technical and engineering support within areas of technical competence is provided to ESD Program Offices (POs) and other ESD elements. The principal technical mission areas are communications, electromagnetic guidance and control, surveillance of ground and aerospace objects, intelligence data collection and handling, information system technology, ionospheric propagation, solid state sciences, microwave physics and electronic reliability, maintainability and compatibility.

4-8